Received: 2 April 2018 | Revised: 24 November 2018 | Accepted: 29 November 2018

DOI: 10.1002/gea.21735

RESEARCH ARTICLE

WILEY Geoarchaeology An International Journal

Late Pleistocene site formation and paleoclimate at Lapa do Picareiro, Portugal

Michael M. Benedetti[1,4] | Jonathan A. Haws[2,4] | Nuno F. Bicho[3,4] | Lukas Friedl[4,5] | Brooks B. Ellwood[6]

[1]Department of Earth and Ocean Sciences, University of North Carolina Wilmington, Wilmington, North Carolina

[2]Department of Anthropology, University of Louisville, Louisville, Kentucky

[3]Faculdade das Ciências Humanas e Sociais, Universidade do Algarve, Campus de Gambelas, Faro, Portugal

[4]Interdisciplinary Center for Archaeology and Evolution of Human Behaviour (ICArEHB), Faculdade das Ciências Humanas e Sociais, Universidade do Algarve, Campus de Gambelas, Faro, Portugal

[5]Department of Anthropology, University of West Bohemia, Plzen, Czech Republic

[6]Department of Geology and Geophysics, Louisiana State University, Baton Rouge, Louisiana

Correspondence
Michael M. Benedetti, Department of Earth and Ocean Sciences, University of NC Wilmington, Wilmington, NC 28403.
Email: benedettim@uncw.edu

Funding information
Division of Behavioral and Cognitive Sciences, Grant/Award Numbers: 1725015, 1724997, 1420453, 1420299

Scientific editing by Jamie Woodward

Abstract

The cave site of Lapa do Picareiro, Portugal contains a deep (~10 m) sedimentary sequence representing much of the Middle and Upper Paleolithic, with abundant animal bones, lithic/bone/shell artifacts, and charcoal/ash in hearths. A deposition model based on 49 radiocarbon ages demonstrates average sedimentation rates of 0.1–0.3 mm a^{-1} between 9 and 45 ka. Extrapolation suggests an age at the base of the excavation of 65–78 ka. The cave sediments are primarily limestone éboulis derived from roof spalling, and muddy fine sediment derived from weathered soil infiltrating through bedrock joints and crevices. Bone preservation in the cave is good and disturbance by bioturbation, dissolution, or erosional processes appears to be limited. Most sedimentological parameters vary conservatively with depth, indicating stable sediment sources over time. Several parameters show good agreement with paleoclimate records over the radiocarbon-dated section. The cold-arid Heinrich stadials are represented by coarse-clast beds with little fine sediment and magnetic susceptibility minima, and mild Greenland interstadials correspond with muddy beds and sharp peaks in magnetic susceptibility. This study complements ongoing archaeological excavation at the site and confirms that the sequence has the proper age, resolution, and preservation to inform on Late Pleistocene cultural and climatic transitions.

KEYWORDS
caves, Iberia, paleoclimate, Paleolithic, site formation

1 | INTRODUCTION

Sedimentary deposits in caves and rock shelters are central to our understanding of human prehistory. Although caves represent only a fraction of the landscapes occupied by prehistoric humans, under the proper conditions they offer long-term preservation of valuable paleoenvironmental information in stratified sedimentary archives. The study of karstic sediments as environmental archives has a strong tradition in geoarchaeology, beginning with seminal works of the last century and advanced by developments in both methodology and theory (e.g., Collcutt, 1979; Bar-Yosef et al., 1992; Ellwood et al., 2004; Farrand, 2001; Gamble, 1986; Goldberg & Sherwood, 2006; Karkanas, Bar-Yosef, Goldberg, & Weiner, 2000; Laville, Rigaud, & Sackett, 1980; Woodward & Goldberg, 2001). Recent geoarchaeological research in caves employs state-of-the-art dating techniques, isotope geochemistry, micromorphology, and spectroscopy to interpret site formation processes over timescales from hundreds of years to hundreds of millennia (e.g., Angelucci & Zilhão, 2009; Berger et al., 2008; Courty & Vallverdu, 2001; Shahack-Gross et al., 2008; Woodward, Hamlin, Macklin, Karkanas, & Kotjabopoulou, 2001; Aldeias et al., 2016; Arriola-bengoa, Iriarte, Aranburu, Yusta, & Arrizabalaga, 2015; Domingo et al., 2015; Goldberg et al., 2012; Gopher et al., 2010; Karkanas & Goldberg, 2010; Mallol, Cabanes, & Baena, 2010; Sanudo, Blasco, &

Fernandez Peris, 2016; Skaberne, Turk, & Turk, 2015; Wood et al., 2014).

Although caves and rock shelters offer certain natural advantages for paleoenvironmental reconstruction, such studies are complicated by the nonlinear response of karst systems to climate change. Sedimentary processes in caves are driven by allogenic factors, such as regional climate and vegetation, and autogenic factors, such as bedrock lithology and development of karst conduits. Climate change simultaneously initiates allogenic and autogenic adjustments, making these causes difficult to untangle without independent evidence from other paleoenvironmental proxies. The situation is further complicated in caves occupied by prehistoric humans, where an observed pattern of human activity (e.g., artifacts) may or may not represent responses to environmental change, and people themselves may serve as a cause of environmental change. Cave-derived records of environmental change and human activity are often incomplete or altered by diagenesis, which itself may be influenced by natural or anthropogenic factors. These relationships complicate geoarchaeological studies in caves, whether the goal is to derive paleoclimate records from sediments, to reconstruct site formation processes, or to infer human activities from archaeological evidence.

For the Paleolithic of the Iberian Peninsula, much of the dated lithic industry and virtually all of the human remains are known from cave and rockshelter sites, such as Gorham's and Vanguard Caves (Macphail & Goldberg, 2000), Atapuerca (Bermudez de Castro et al., 2004), El Mirón (Carretero et al., 2015), El Sidrón (Lalueza Fox, Rosas, & de la Rasilla, 2012; Rosas et al., 2006), Cueva del Esquilleu (Presleyer et al., 2012), El Castillo (Bernaldo de Quiros et al., 2015), the Almonda cave network (Angelucci & Zilhão, 2009; Daura et al., 2017; Trinkaus, Maki, & Zilhão, 2007), Vale Boi (Bicho et al., 2013), and many others (Butzer, 1981; Duarte et al., 1999; Zilhão et al., 2010; Carbonell, 2012; de la Torre, Martinez-Moreno, & Mora, 2013; Zilhão et al., 2016; Zilhão et al., 2017;Trinkaus & Walker, 2017). Iberian cave and rockshelter sites play an important role in a number of contemporary debates in Paleolithic Geoarchaeology, including the emergence of coastal adaptations and settlement (Bicho & Haws, 2008; Finlayson, 2008; Haws et al., 2010; Marean, 2014; Stringer et al., 2008), the impacts of paleoenvironmental fluctuations on cultural transitions (Bicho, Cascalheira, Marreiros, & Pereira, 2017; Bicho, Haws, & Almeida, 2011; Mallol, Hernandez, & Machado, 2012; Moreno, Gonzalez-Samperiz, Morellon, Valero-Garces, & Fletcher, 2012; Naughton et al., 2009; Schmidt et al., 2012), and the causes of Neanderthal decline and replacement by Modern Human populations (Aubry et al., 2011; Bicho, 2005; Finlayson & Carrion, 2007; Finlayson et al., 2006; Galvan et al., 2014; Higham et al., 2014; Jimenez-Espejo et al., 2013; Marin-Arroyo et al., 2018; Mora et al., 2018; Polo-Diaz, Benito-Calvo, Martinez-Moreno, & Mora Torcal, 2016; Straus, Bicho, & Winegardner, 2000; Tzedakis, Hughen, Cacho, & Harvati, 2007; Wood et al., 2013; Zilhão et al., 2010). Iberia has many favorable characteristics for supporting cave-based studies of Paleolithic human-environment interactions, including several large limestone provinces, a climate-sensitive location between the Eurosiberian and Mediterranean ecosystems, and excellent paleoenvironmental proxy records from offshore sediment cores (Roucoux, de Abreu, Shackleton, & Tzedakis, 2005; Turon, Lezine, & Denefle, 2003; Vautravers & Shackleton, 2006; García-Amorena et al., 2007; Sánchez Goñi et al., 2008; Fletcher et al., 2010; Gonzalez-Samperiz et al., 2010; Salgueiro et al., 2010).

Unfortunately, many Iberian cave sequences are hindered by poor age control and stratigraphic resolution, especially at sites that define key transitions in the Paleolithic. Late Pleistocene climate fluctuations caused impacts that either changed the conditions under which Paleolithic populations acted, or destroyed archaeological evidence of those populations, or both. Such climate-driven impacts include shifting flora and fauna (Blain et al., 2013; Carrión & Leroy, 2010; Domingo et al., 2015; Fletcher et al., 2010; Haws, 2012; Straus, 2013), rapid changes in human population dynamics, and settlement patterns (Bicho et al., 2017; Brädtmoller, Pastoors, Weninger, & Weniger, 2012; Cucart-Mora, Lozano, & Fernandez-Lopez de Pablo, 2018; Finlayson & Giles Pacheco, 2000; Schmidt et al., 2012; Zilhão, 2000), and changes in the availability of abiotic resources (Pereira & Benedetti, 2013). Most notably, Heinrich stadial 4 (HS4; roughly 38–40 ka) has been cited as a cold/arid episode that drastically altered environmental conditions, playing a possible role in Neanderthal extinction but also causing geological impacts that obscured evidence of the Middle to Upper Paleolithic transition (Aubry et al., 2011; d'Errico & Sanchez Goñi, 2003; Finlayson & Giles Pacheco, 2000; Zilhão, 2006; Bradtmöller et al., 2012; Mallol et al., 2012; Schmidt et al., 2012). Other authors have highlighted the difficulties with establishing reliable radiocarbon chronologies to address cultural transitions in the Paleolithic (Blockley, Ramsey, & Higham, 2008; Jöris & Street, 2008; Higham, 2011; Morley & Woodward, 2011; Banks, 2015; Douka & Higham, 2017; Wood et al., 2013). These studies demonstrate that further progress in the Iberian Paleolithic depends on discoveries from new high-resolution sites with stratigraphic integrity, firm age control, and correlations with existing land and ocean-based proxies.

This paper reports on sedimentological studies that complement the ongoing archaeological excavation of Lapa do Picareiro (Picareiro Cave) near Fátima, Portugal. The cave contains a Late Pleistocene sedimentary sequence representing much of the Middle and Upper Paleolithic, recording evidence of changing human populations, lithic industries, paleoenvironments, and faunal communities. The data presented here are based on field observations and mapping, radiocarbon ages, and analysis of particle size, composition, magnetic susceptibility (MS), elemental geochemistry, and stable isotope ratios. The primary goals of this paper are to (a) establish a chronology of site formation for Lapa do Picareiro, (b) shed light on modes of deposition for various components of the sedimentary fill of the cave, and (c) assess the value of evidence from Lapa do Picareiro for paleoenvironmental reconstruction and correlation with other regional paleoclimate proxies. These results help to demonstrate the stratigraphic integrity and completeness of the site and develop a geological framework for ongoing archaeological and archaeofaunal studies.

2 | LAPA DO PICAREIRO: ENVIRONMENTAL AND ARCHAEOLOGICAL CONTEXT

Lapa do Picareiro is located at 570 msl on the west-facing slope of Serra de Aire, a limestone massif north of the Tagus River valley, about 100 km northeast of Lisbon, Portugal (Figure 1). The massif is underlain by the Serra de Aire Formation, a thickly-bedded, micritic limestone of Middle Jurassic age (Carvalho, 2018). Serra de Aire is part of a large limestone province in west-central Portugal (Maciço Calcário Estremenho) that includes many well-known caves and rock shelters, some of which contain important Paleolithic archaeological sites, such as Buraca Escura (Aubry et al., 2001), Buraca Grande (Aubry, Fontugne, & Moura, 1997), Lapa do Anecrial (Almeida, Brugal, Zilhão, Plisson, & Bicho, 2007), and Lagar Velho (Almeida, Moreno-Garcia, & Angelucci, 2009; Zilhão & Almeida, 2002). Two other large cave systems lie in the immediate vicinity of Serra de Aire: The archaeologically-sterile Grutas da Mira de Aire and the Almonda karst system. Almonda contains several important Middle and Late Pleistocene sites including Galeria Pesada (Gruta da Aroeira) and Gruta da Oliveira, both with human remains, and Lapa dos Coelhos (Angelucci & Zilhão, 2009; Daura et al., 2017; Hoffmann, Pike, Wainer, & Zilhão, 2013; Marks et al., 2002; Trinkaus et al., 2007).

Serra de Aire has a Mediterranean climate with warm dry summers and cool wet winters. The nearby city of Fátima has a mean annual temperature of 14.6°C and precipitation around 920 mm a^{-1} (Cunha et al., 2011). The west-facing mountain summit location of Lapa do Picareiro increases its exposure to strong winds and cold temperatures relative to the surrounding valleys. Modern vegetation includes a mosaic of evergreen oak thickets and dense maquis of aromatic shrubs and herbs (Costa, Espírito Santo, & Arsénio, 2010). Soils formed on limestone in this region are of the "Red Mediterranean" variety of terra rossa (Dudal, Tavernier, & Osmond, 1966), and qualify as haploxeralfs or haploxerepts according to US Soil Taxonomy (Soil Survey Staff, 1999). Paleoenvironmental studies show that during the last glacial stage much of Portugal alternated between periods of increasing temperate forest cover during humid

FIGURE 1 Location of Lapa do Picareiro and nearby sites discussed in the text [Color figure can be viewed at wileyonlinelibrary.com]

interstadials, and increasing dry grassland or steppe during cold and arid stadials (Sánchez Goñi et al., 2008; Fletcher et al., 2010). Snow and frost are infrequent in the modern climate but were presumably common during the Pleistocene.

The interior of Lapa do Picareiro is a large chamber, about 11 × 14 m with a wide mouth opening to the northwest and several narrow side passages in the interior walls (Figures 2 and 3). The cave has most of the properties of a passive karst setting (*sensu* Woodward & Goldberg,

FIGURE 2 Photographs of the cave and sedimentary fill. (a) Aerial view of the opening of Lapa do Picareiro near the summit of Serra de Aire, view to the southwest; (b) ground-level view of the cave entrance with exposed bedrock dipslope above the cave opening, view to the east; (c) view of the cave interior during excavation in 2016; main excavation area fills the lower half of the photo, niche area is visible in the top center; (d) profile view of levels T-JJ showing semiperiodic variations in clast size and mud content in the main excavation area (units E11 and E12); (e) profile view of zone 1 sediments in the vicinity of reference profile 1, including light-colored ash and charcoal-rich sediments in level E, dark Magdalenian hearth in level F, and large clasts with little fine sediment in levels I-J; (f) speleothems covering the cave wall in the niche area (unit XX11); flowstone emerges from a sealed opening in the bedrock, covering and cementing level F at the surface; hand pick is 35 cm long; (g) crevice in the cave wall exposed by excavation, with reddish-brown mud filling the lower half of the crevice and spilling into the cave fill at level K (unit ZZ6); width of crevice opening is about 40 cm [Color figure can be viewed at wileyonlinelibrary.com]

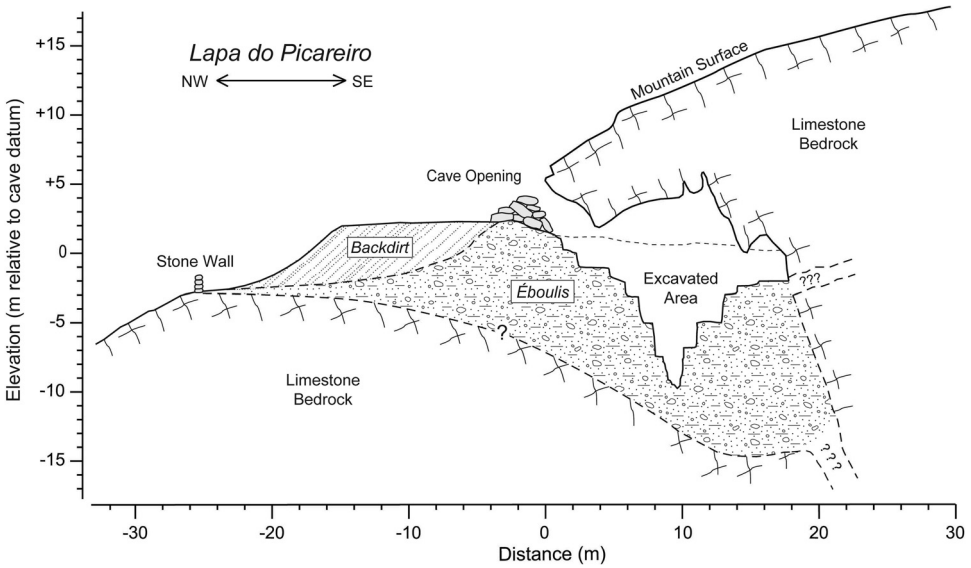

FIGURE 3 Generalized cross section of Lapa do Picareiro showing surface topography, shape of the cave, and area excavated into sedimentary fill

2001): little or no vegetation growth, no flowing water, lack of obvious links to internal karst conduits, and limited chemical diagenesis. Active karst properties include localized precipitation of secondary carbonates and evidence for fine sediment infiltration through bedrock joints and crevices. The cave appears to have a simple epigenetic origin, formed by diffuse infiltration of meteoric water through the overlying bedrock leading to the dissolution of the main chamber and roof collapse to form the cave entrance. The cave also fits the definition of an aging chamber cave (*sensu* Frumkin et al., 2009), with more than 10 m of coarse sedimentary fill in inclined beds derived from roof collapse, gravity flows, and fine sediment infiltration. A cone of large limestone blocks below the dripline nearly filled the cave opening (Bicho, Haws, & Hockett, 2006), whereas sediments inside the main chamber consist of angular limestone clasts (éboulis) in a matrix of fine sediment (dominantly silt and clay).

Archaeological studies at Picareiro since 1994 have uncovered a rich variety of lithic artifacts and faunal remains. Previously published data from this work include MS measurements, radiocarbon ages, analysis of faunal and lithic assemblages, and site stratigraphy for the Upper Paleolithic levels (Hockett & Bicho, 2000; Ellwood et al., 2001; Bicho, Hockett, Haws, & Belcher, 2000; Bicho et al., 2006; Hockett & Haws, 2002, 2009; Haws, 2012; Benedetti & Haws, 2016; Haws et al., 2018). Through 2017, more than 120 m^2 units have been opened and 40 stratigraphic levels (A through NN) have been identified to a depth of more than 10 m (Figures 4 and 5). Bone, shell, and charcoal preservation in the cave sediments is very good. Many thousands of bones have been recovered, predominantly rabbit and red deer with lesser frequencies of wild boar, ibex, horse, auroch, and chamois. Fauna also includes abundant bird, amphibian, and fish remains.

The Paleolithic archaeological findings at Lapa do Picareiro occupy two main areas: (a) A thick sequence of Middle to Upper Paleolithic occupations in the main excavation area of the main chamber (centered on units E7-F8, Figure 5) and (b) Upper Paleolithic occupations found in a niche in the rear wall (units XX9-ZZ11, Figure 5). Additional Epipaleolithic, Neolithic, and Bronze Age occupations were found in disturbed sediments near the cave entrance (Bicho et al., 2006), but these levels were not sampled as part of the present study. The dominant Upper Paleolithic feature discovered in the main excavation area is a large Magdalenian hearth in level F (Figure 2e), rich in lithics and modified faunal remains, from which Bicho et al. (2006) concluded the site was used mainly for butchering and cooking animal carcasses. A series of stacked hearths in the niche area date to the Magdalenian, Solutrean, proto-Solutrean, and Terminal Gravettian. Magdalenian levels in the niche area (I, J, K, L) contained pointed/incised bone tools, chert blades and bladelets, and abundant ungulate and rabbit remains (Figure 6). The Solutrean levels (N, O, R, S, and upper part of T) contained bifacial points, perforated shell, bone points, and an eyed bone needle. The middle portion of level T contained several small hearth features with associated chert blanks, consistent with a Proto-Solutrean industry (as discussed in Zilhão, 2013; Cascalheira & Bicho, 2015), along with bone tools and marine shell pendants. The Terminal Gravettian assemblage (lower level T and U) consists of quartz and chert bladelets, bone tools, and perforated red deer canine teeth. Deeper layers of the main excavation area contain a Gravettian-aged lithic assemblage (levels V, W, X) dominated by quartzite flakes associated with dispersed charcoal and abundant fauna, including extremely rich concentrations of small animal bones (Haws, 2012). Large mammal bones in these levels display both intentional breakage and cut marks by humans, and tooth punctures and scoring attributed to larger predators including lynx. Early Upper Paleolithic flake and blade industries occur in the back of the cave in levels BB, DD, and FF to II. This includes large chert flakes and blades in levels BB and DD, quartz and quartzite flakes in level FF, and a diagnostic Aurignacian chert bladelet assemblage in levels GG-HH-II (Haws et al., 2018). In the main excavation area, Level FF contains a flake core, sidescraper, and several undiagnostic flakes. Level JJ contains the youngest definitive Middle Paleolithic occupation, with discoidal flakes

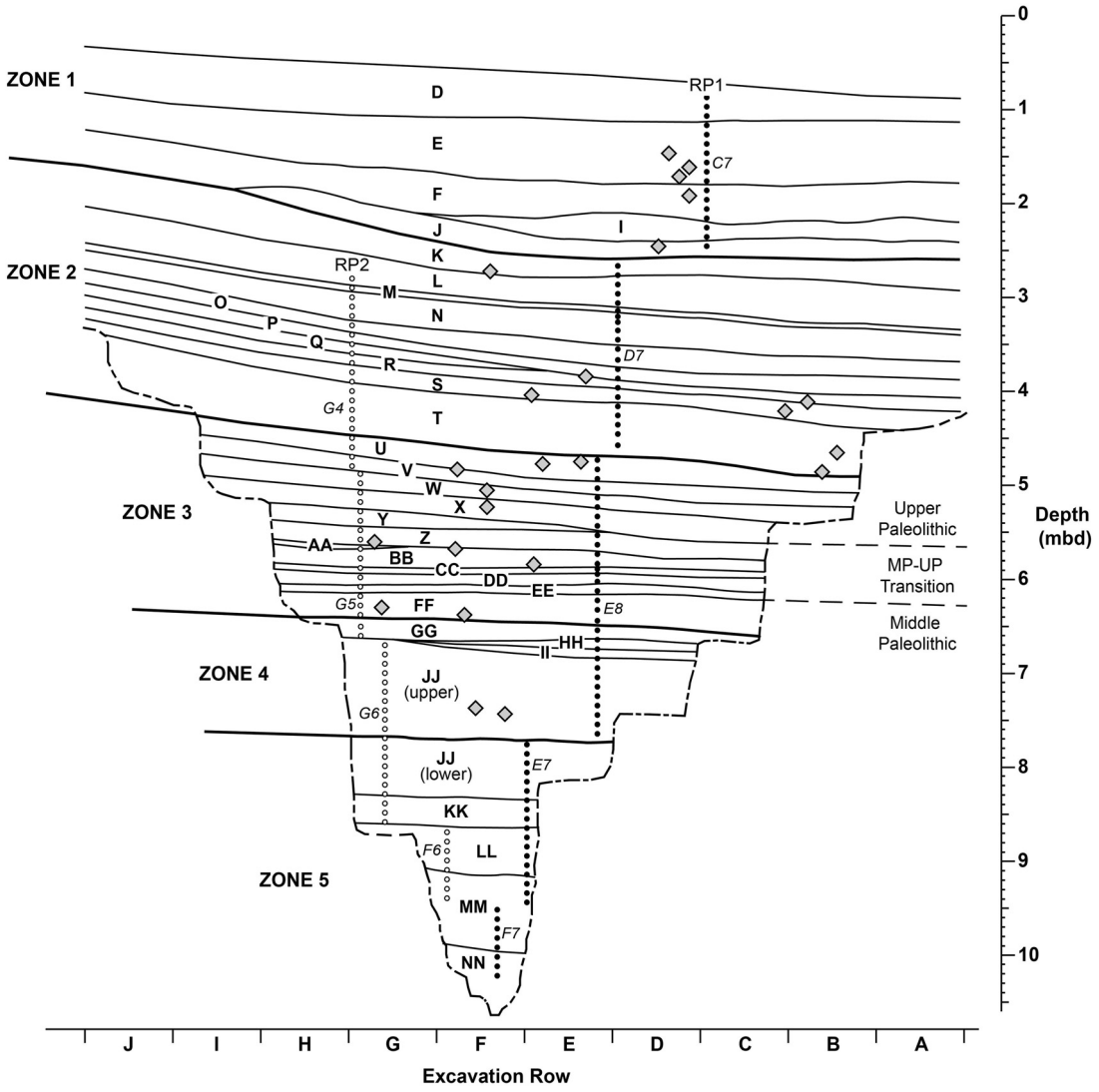

FIGURE 4 Stratigraphic profile of excavated levels D to NN, which were exposed at different times in stepped profiles along rows 5, 6, and 7. View is to the northeast in the main excavation area. Also shown are the locations of reference profile samples (dots) and radiocarbon samples (diamonds) collected from this part of the cave. Reference profile 1 (RP1, black dots) and reference profile 2 (RP2, white dots) are labeled with the row from which each section of samples was collected. The large Magdalenian hearth that dominates the sedimentological properties near the top of the section was excavated in level F (Bicho et al., 2006)

occurring in several dark layers that also contain abundant charcoal and fauna. Only 2 m^2 units have been excavated into the deepest levels (KK-NN); these contain some small animal bones but no artifacts to this point. Collectively, the archaeological evidence at Picareiro demonstrates periodic but increasing human use of the cave beginning in the Middle Paleolithic and continuing through the Upper Paleolithic to a climax in the Magdalenian.

3 | METHODS

The archaeological excavation at Lapa do Picareiro follows a traditional 1 × 1 m grid system. Stratigraphic levels have been assigned during excavation on the basis of changes in clast size, color, mud content, firmness, and bone or charcoal concentrations. The 40 levels identified to date are divided here into 5 stratigraphic zones (similar to facies associations) based on macroscopic field and laboratory sedimentological properties. Mapping of stratigraphic levels, artifacts, features, and cave morphology have been achieved by three-dimensional plotting with a total station and complemented by annual terrestrial laser scanning of the cave and its surroundings. Elevations in and around the cave are tied to a vertical datum (571 m above sea level) that was established slightly above the original sediment surface. Elevation data presented in this paper are reported relative to this level as meters below datum (mbd).

For geoarchaeological analyses, sediment samples were collected at approximately 10-cm depth intervals from the top of the section in two stepped reference profiles (locations shown in Figures 4 and 5) over several field seasons. Most data in this study were collected from reference profile 1 near the rear wall of the main excavation

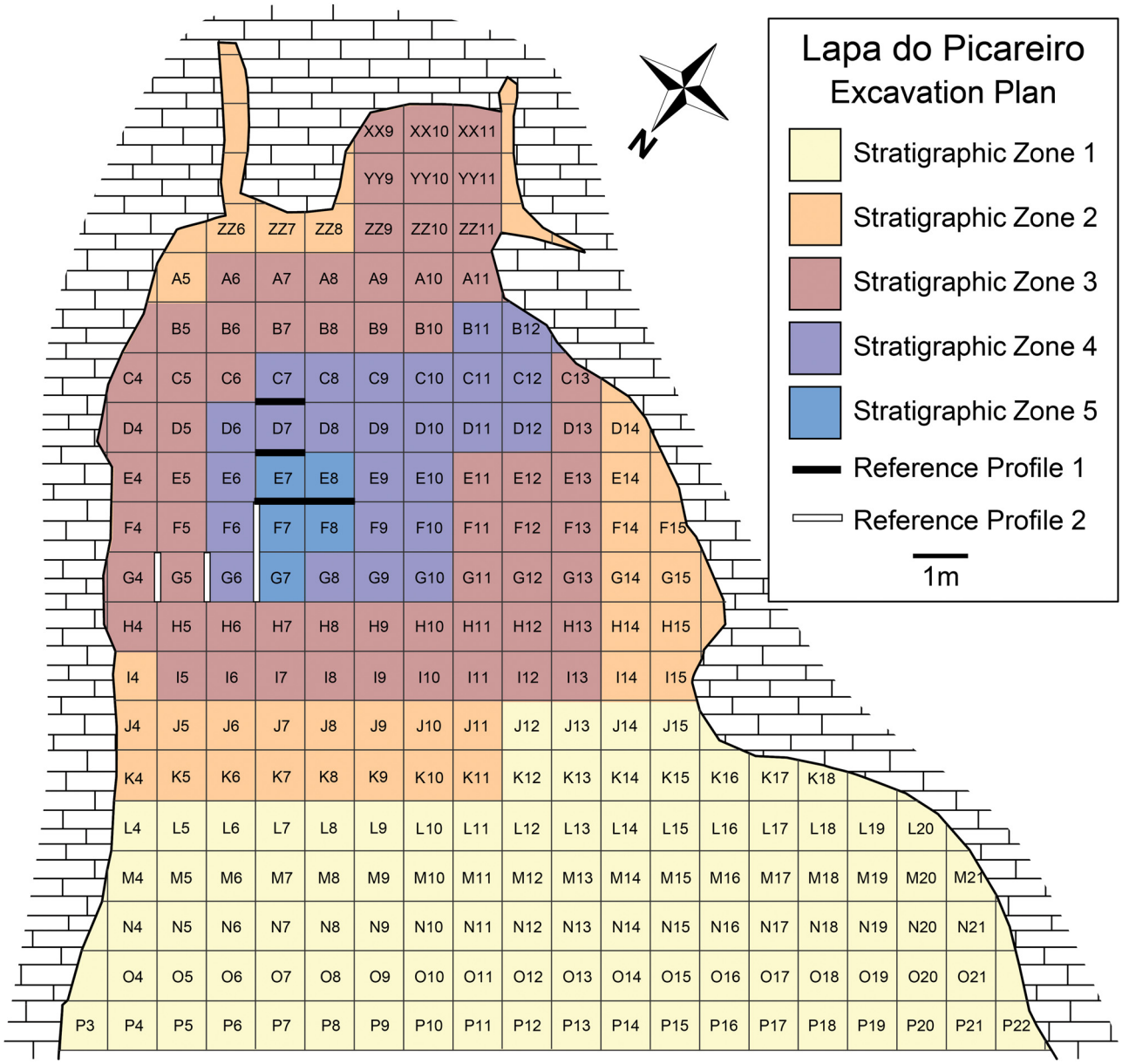

FIGURE 5 Excavation plan for Lapa do Picareiro showing the dimensions of the cave interior, stratigraphic zones exposed as of 2017, and location of the stepped reference profiles that were sampled for sedimentological analyses [Color figure can be viewed at wileyonlinelibrary.com]

area, extending from level D to NN (0.87–10.20 mbd). Additional samples were collected along the north wall of the main excavation area in reference profile 2, extending from level L to MM (2.80–9.38 mbd). The second profile was established to help characterize changes in the sedimentary strata with distance from the mouth of the cave. The 10-cm sampling interval was the finest resolution practical without disrupting the archaeological profiles, given that most beds contain very little fine sediment. Additional targeted bulk samples were collected from cemented layers, blocks of in situ limestone bedrock, weathered limestone clasts in the sedimentary fill, fine sediment filling cracks in the cave wall, and soil pits described on the surface outside the cave.

Field description of the reference profiles included bed thickness, strike/dip, color, hardness, percent éboulis (clasts >2-mm long axis) versus fine sediment matrix, clast size, and roundness. We used two techniques to characterize éboulis clast size. First, to characterize typical clast sizes we assigned a modal clast size category (very small to very large) to each level during excavation. Second, to more precisely characterize the finely-bedded coarse and fine éboulis layers, we measured the long axis of the largest 5 éboulis clasts visible in each 10 cm depth horizon of a 1-m wide profile wall. We then calculated the mean size of these clasts, a result referred to below as mean large clast size (in mm). This method allowed for a relatively fast and noninvasive means of representing clast size variations at the two reference profiles. Large boulders (long axis >500 mm) were not encountered in the immediate area of the reference profiles, except in the very deepest level (NN). Levels with significant boulder concentrations

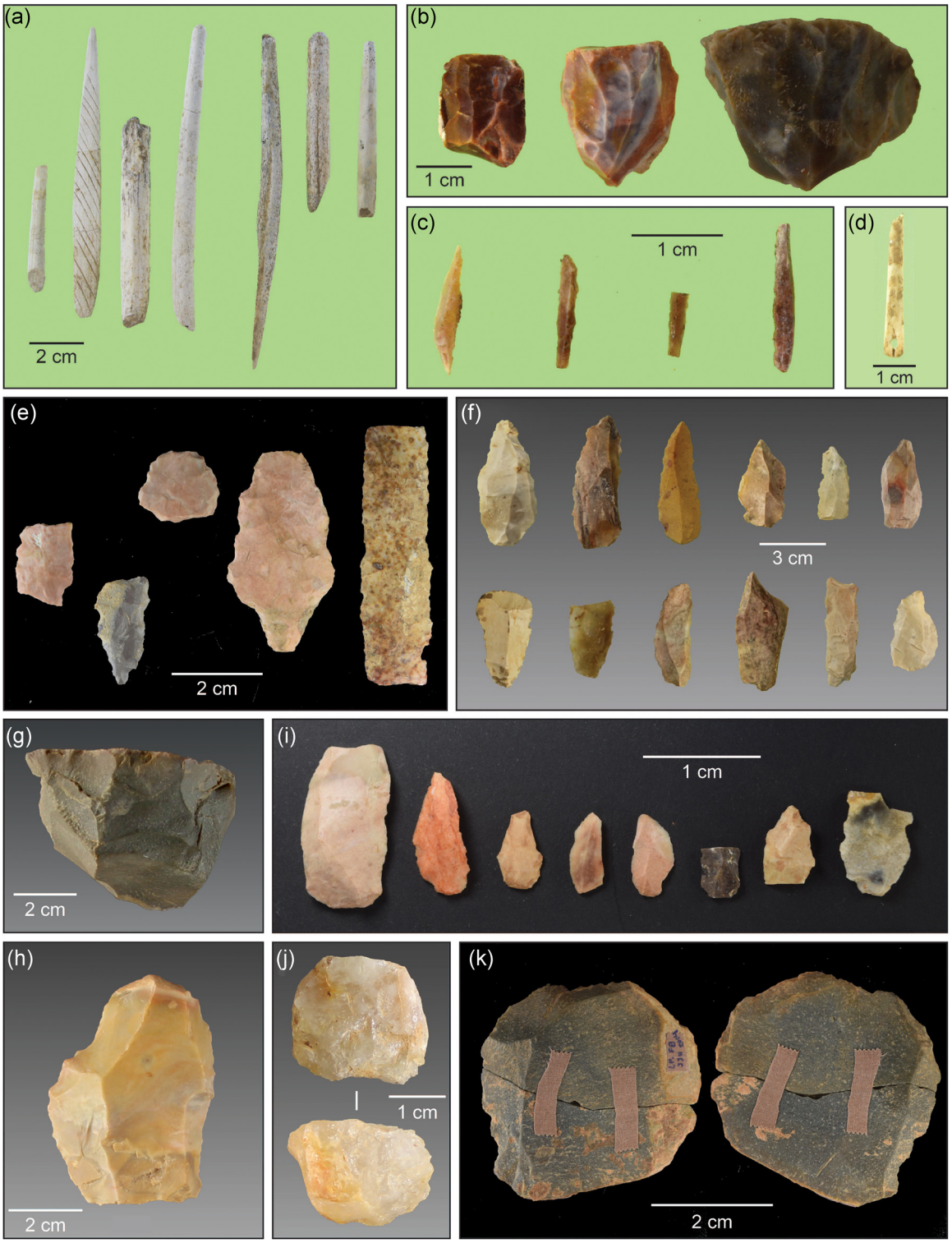

FIGURE 6 Photographs of artifacts recovered in the excavation of Lapa do Picareiro. (a) Magdalenian bone tools from the niche area, levels K-L; (b) Magdalenian chert bladelet cores, levels I-K; (c) Magdalenian chert bladelets, levels I-K; (d) Solutrean eyed bone needle from the niche area, level T; (e) Solutrean chert bifacial points, levels R-T; (f) Solutrean or Proto-Solutrean chert blades, levels S-T; (g) Gravettian quartzite core, level W; (h) Gravettian chert end scraper, level W; (i) Aurignacian bladelets, levels GG-HH-II; (j) quartz core, level FF; (k) refit of Mousterian discoidal quartzite flake, level JJ [Color figure can be viewed at wileyonlinelibrary.com]

elsewhere in the cave were noted and mapped throughout the excavation.

Sedimentological analyses were completed on the <2 mm fraction of the profile samples at the UNC Wilmington Soils & Sedimentology Laboratory. Particle size was measured by laser diffraction (Beckman Coulter LS 13320) on samples that had been pretreated with 30% hydrogen peroxide to remove organic matter and dispersed in sodium metaphosphate. Organic matter and carbonate content (weight %) were estimated for both profiles by loss on ignition (LOI) in a muffle furnace at 2.5 hr at 550°C for organic matter and 4 hr at 950°C for carbonates. Stable isotopes ($\delta^{13}C$ and $\delta^{15}N$), along with organic carbon and nitrogen concentrations, were measured for Profile 1 samples by a mass spectrometer (Thermo Scientific DELTA V Plus) coupled with an elemental analyzer at the UNC Wilmington Isotope Ratio Mass Spectrometry Facility. The isotope samples were pretreated in a 10% HCl bath and rinsed at least three times to remove secondary carbonates before analysis, and repeated analyses of USGS standards were used to ensure high precision (see Lane, Horn, Mora, & Orvis, 2009). Although the organic matter was limited in some parts of the profile, all samples analyzed had readily measurable concentrations of organic carbon 0.16–19.62%) and nitrogen 0.03–0.55%) and thus produced reliable isotope ratios. Samples from both profiles were also analyzed for lithogeochemistry by inductively coupled plasma optical emission spectrometry at Activation Laboratories Ltd. in Ancaster, Canada. This analysis provided concentration data for 10 major earth compounds (SiO_2, Fe_2O_3, Al_2O_3, CaO, MnO, MgO, TiO_2, Na_2O, K_2O, P_2O_5 in weight %) and seven trace elements (Ba, Sr, Y, Sc, Zr, Be, V in ppm). Less-abundant compounds and elements are reported here as ratios standardized to the concentration of TiO_2 (MnO/TiO_2, P_2O_5/TiO_2, Zr/TiO_2, Sr/TiO_2) to reduce the dilution effect in levels that are strongly enriched in secondary carbonates.

A parallel set of samples were collected adjacent to reference profile 1 for MS analysis. These samples were collected beginning in 2000, and continuing as the excavation was deepened. For this analysis, approximately 8 cm^2 of fine sediment was collected in plastic boxes to standardize sample size and exclude large limestone clasts. Most of the profile was sampled at 2 cm depth intervals, although the interval is greater (up to 5 cm) in strata containing very little fine sediment. One 30-cm thick bed consisting almost entirely of coarse clasts (Level J) was not sampled. Although the bulk samples from reference profile 1 extend to 10.20 mbd, the MS sampling profile extends to the base of the deepest excavation at 10.62 mbd. MS was measured using the susceptibility bridge at Louisiana State University, described in Ellwood et al. (1998). Data from the early sampling campaign were published in Ellwood et al. (2001), which also describes the analytical procedures used, discusses the interpretation of MS in cave settings, and compares the magnetic stratigraphy of several cave sequences across Mediterranean Europe.

Age control for the sedimentary sequence at Lapa do Picareiro comes from radiocarbon dating of 56 samples of charcoal and bone (Table 1). These samples were collected to establish the age of archaeological features and stratigraphic levels throughout the excavation. Depths were mostly measured in situ during excavation, except for bulk charcoal samples collected from excavation spits that are associated with a 5–10 cm depth range. Most of the radiocarbon samples were collected in the main excavation area between rows 5–9 and rows B to G (Figure 5). Every sample below level X was collected from the main excavation area. The samples were analyzed at three different radiocarbon laboratories as the excavation progressed (Waikato Radiocarbon Dating Lab, University of Georgia Center for Applied Isotope Studies, and Beta Analytic, Inc.). The bone samples analyzed most recently at Waikato have been treated by the well-documented ultrafiltration method that reduces potential contamination and provides more accurate age determinations (Bronk Ramsey, Higham, Bowles, & Hedges, 2004; Talamo et al. 2012). These samples contain 37–45% organic carbon and have C:N ratios within the range of 3.0–3.5, indicating good preservation of bone collagen (Table 1). Other samples have received more traditional sample treatments, such as the acid-base-acid method for charcoal (Brock, Higham, Ditchfield, & Bronk Ramsey, 2010).

4 | RESULTS

4.1 | Field descriptors

The sedimentary fill of Lapa do Picareiro is primarily composed of limestone éboulis clasts in a matrix of grayish to reddish-brown muddy fine sediment (Figure 2d,e). In the main excavation area that is the focus of this study, bedding alternates between muddy levels with 20–40% fine sediment and gravelly beds with little or no fine sediment (Table 2). Boundaries between the beds are gradual and smooth, with little or no evidence for erosional unconformities or postdepositional disturbance. Most beds are clast-supported, and virtually all clasts (small éboulis to boulders) are angular to subangular, with roughly equidimensional to slightly elongated shapes showing very little evidence of postdepositional weathering. Clast size is moderately well-sorted within each level and tends to alternate between coarse-clast and fine-clast levels, indicative of periodic variations in the weathering environment. The beds dip gently eastward away from the cave mouth and have a slight upward concavity, whereas the clast size within each bed tends to decrease toward the rear of the cave. Although not prevalent, some muddy beds contain large clasts floating within a fine matrix and imbricated clasts suggesting mobilization by small-scale debris flows (Karkanas & Goldberg, 2016). Dip measurements on coarse beds in the vicinity of reference profile 2 show that the upper beds dip more steeply into the cave (levels N, P, T; 10–12° inclination) than the lower beds (levels V, Y, BB, GG; 2–4°), consistent with a ramp of éboulis prograding toward the back of the cave over time. Large boulders are scattered sporadically throughout the sedimentary fill but are concentrated in a rockfall cone beneath the cave entrance, where randomly-oriented blocks have accumulated after detaching from an exposed bedrock dip slope above the cave opening (Figures 2 and 3).

Sediments near the cave mouth are darker and more organic-rich than sediments in the cave interior and show moderate to strong

TABLE 1 Radiocarbon ages and complementary data from the excavation of Lapa do Picareiro

Level	Unit	Depth, mbd[a]	Lab number	Sample material	Radiocarbon age (^{14}C yr BP)	Cal 2σ range (cal yr BP)[b]	δ^{13}C (‰)	%C	C:N
B	I5	0.75	UGAMS-9099	Charcoal	8,700 ± 30	9,735–9,550	−24.5		
B	C5	0.85	UGAMS-9098	Charcoal	8,500 ± 30	9,535–9,475	−25.0		
C	E12	1.10–1.15	Wk-41388[c]	Bone	10,720 ± 40	12,727–12,589	n/a[g]		
D	G4	1.15–1.25	Wk-6676[d]	Charcoal	8,310 ± 130	9,528–9,014	−25.2		
E	D6	1.45–1.50	Wk-4217[d]	Charcoal	10,070 ± 80	11,980–11,307	−24.2		
E	D6	1.60–1.65	Wk-5431[d]	Charcoal	11,700 ± 120	13,764–13,296	−24.7		
E	D6	1.70–1.75	Wk-4218[d]	Charcoal	11,550 ± 120	13,605–13,119	−24.3		
F	D8	1.85–1.90	Wk-10434[d]	Charcoal	12,500 ± 160	15,228–14,110	−23.1		
F	D6	1.90–1.95	Wk-4219[d]	Charcoal	11,780 ± 90	13,772–13,442	−24.7		
F	F5	2.15–2.20	Wk-6677[d]	Charcoal	12,210 ± 100	14,607–13,778	−24.3		
F	ZZ10	2.29	UGAMS-20480	Charcoal	11,760 ± 30	13,719–13,467	−25.2		
F	ZZ9	2.40	Wk-41257[c]	Bone	12,260 ± 30	14,323–14,028	−20.8	37.67	3.47
J	D7	2.40–2.45	Wk-6678[d]	Charcoal	11,880 ± 80	13,950–13,485	−24.1		
J	D5	2.90–2.95	Wk-10433[d]	C harcoal	10,490 ± 110	12,678–12,052[f]	−24.3		
J	D5	3.10	WK-12129	Bone	12,120 ± 70	14,150–13,777[f]	−20.8		2.97
K	F6	2.71	Wk-31354[c]	Bone	15,040 ± 90	18,512–18,006	−20.7	41.99	3.38
L	E9	2.82	UGAMS-17664	Charcoal	15,680 ± 40	19,035–18,800	−23.7		
N	D5	3.32	Wk-16417[e]	Bone	16,390 ± 110	20,070–19,511	−20.1	13.70	3.52
O	G9	3.00	Beta-247965[e]	Charcoal	17,480 ± 100	21,450–20,805	−24.4		
O	YY11	3.40	UGAMS-23724	Charcoal	16,280 ± 40	19,854–19,497	−24.3		
O	YY10	3.68	UGAMS-24606	Charcoal	17,570 ± 50	21,451–21,002	−22.8		
R	E6	3.83	Beta-234370	Charcoal	8,670 ± 40	9,732–9,541[f]	−25.0		
R	E7	3.85	UGAMS-03415[e]	charcoal	19,100 ± 70	23,335–22,758	−24.3		
R	B7	4.12	UGAMS-23719	Charcoal	19,090 ± 50	23,272–22,772	−25.1		
S	E6	4.06	Beta-234371[e]	Charcoal	19,290 ± 80	23,510–22,965	−24.4		
S	B7	4.20	UGAMS-23720	Charcoal	18,930 ± 50	23,001–22,569	−24.4		
T	F8	4.21	Wk-37655[c]	Bone	18,960 ± 80	23,069–22,551	−20.3	43.67	3.22
T	YY11	4.46	UGAMS-23725	Charcoal	20,320 ± 50	24,586–24,177	−25.0		
T	B9	4.49	UGAMS-23718	Charcoal	20,240 ± 50	24,508–24,104	−23.7		
T	YY11	4.51	UGAMS-23726	Charcoal	20,530 ± 50	24,999–24,437	−22.9		
T	XX12	4.56	UGAMS-23727	Charcoal	19,530 ± 50	23,761–23,276	−26.0		
T	E5	4.55–4.60	Beta-229781[e]	Bone	20,700 ± 100	25,276–24,545	−21.0		
T	E5	4.55–4.60	Beta-208221[e]	Charcoal	20,240 ± 110	24,615–23,984	−23.6		
T	B7	4.66	UGAMS-23721	Charcoal	20,710 ± 60	25,248–24,615	−22.6		
T	E7	4.86	Wk- 37656	Charcoal	23,100 ± 130	27,641–27,146	−23.8		
T	B7	4.88	UGAMS-23722	Charcoal	20,630 ± 60	25,146–24,530	−23.3		
U	F6	4.88	Beta-234373[e]	Charcoal	22,560 ± 110	27,220–26,525	−23.1		
U	E6	4.90–4.95	Beta-208222[e]	Charcoal	22,660 ± 240	27,461–26,395	−26.1		
U	F6	5.05	Beta-234374[e]	Charcoal	22,590 ± 110	27,246–26,550	−23.8		
V	F6	5.25	Wk-31353[c,e]	Bone	25,580 ± 170	30,320–29,254	−20.2	44.27	3.31
W	F8	5.16	Wk-30539[c,e]	Bone	26,510 ± 270	31,164–30,184	−19.4	42.30	3.20
X	D10	5.16	UGAMS-23723	Charcoal	27,230 ± 80	31,331–30,996	−24.2		
Y	E9	5.63	Wk-41389[c]	Bone	28,430 ± 210	33,041–31,633	−19.0	41.04	3.29
Z	F7	5.60–5.65	UGAMS-03417	Bone	22,190 ± 80	27,076–26,167[f]	−20.3		

(Continues)

TABLE 1 (Continued)

Level	Unit	Depth, mbd[a]	Lab number	Sample material	Radiocarbon age (^{14}C yr BP)	Cal 2σ range (cal yr BP)[b]	δ^{13}C (‰)	%C	C:N
Z	G6	5.64	Wk-32280[c]	Bone	29,050 ± 220	33,769–32,690	−19.4	43.48	3.24
Z	F6, F7	5.73	Wk-30538[c,e]	Bone	28,160 ± 330	32,984–31,307	−19.6	43.50	3.30
BB	E7	5.92	Wk-32281[c]	Bone	30,030 ± 210	34,512–33,745	−19.4	42.93	3.24
FF	F9	6.10	UGAMS-20479	Charcoal	32,200 ± 90	36,355–35,800	−24.0	57.04	
FF	E9	6.25	Wk-41259	Charcoal	33,240 ± 420	38,524–36,381	n/a[g]		
FF	F7	6.25–6.35	Beta-247964[e]	Charcoal	28,610 ± 300	33,485–31,705[f]	−22.3		
FF	F7	6.40	Wk-32219[c]	Bone	33,000 ± 260	38,086–36,355	−19.3	43.02	3.25
FF	F7	6.44	Wk-28843[e]	Bone	27,720 ± 260	32,291–31,087[f]	n/a[g]		
GG	G6	6.33	Wk-41258[c]	Bone	32,060 ± 340	36,726–35,173	−19.0	38.74	3.44
JJ	F7	6.90–7.00	UGAMS-03416	Bone	24,160 ± 100	29,369–28,540[f]	−19.6		
JJ	F7	7.44	Wk-28844[c]	Bone	40,100 ± 1200	46,381–42,094	−19.9	39.53	3.40
JJ	F7	7.50	UGAMS-07769	Charcoal	41,480 ± 220	45,420–44,451	−25.1	55.54	

[a]Sample depths below datum measured by total station. Depth ranges given for samples collected from screens.
[b]Calibrated in OxCal software using IntCal13 calibration curve (Reimer et al., 2013).
[c]Bone samples pretreated with ultrafiltration method (Talamo & Richards, 2011).
[d]Radiocarbon ages previously reported in Bicho et al. (2006).
[e]Radiocarbon ages previously reported in Haws (2012).
[f]Outlier samples not included in deposition model, likely contaminated by carbon from overlying levels.
[g]Insufficient sample size for δ^{13}C determination.

evidence of bioturbation by burrowing animals and plant roots. Most of the burrowing appears to be related to small fauna including rabbits, mice, moles, and insects. Large burrowing animals (such as badger or hyena) are known from Pleistocene assemblages in the region but have not been identified at Picareiro. Sediments inside the main chamber, where the reference profile samples were collected and where most archaeological evidence has been recovered, have smaller clast sizes with more uniform bedding. Most concentrations of charcoal, lithic artifacts, and bones excavated in the cave interior are thin, discrete lenses, suggesting very little diffusion by frost processes or bioturbation. Minor exceptions occur along the walls of the cave interior, where organic debris is often mixed with older sediments in thin (<20 cm) burrowed horizons.

The few speleothems found in Lapa do Picareiro are restricted to small stalactites/stalagmites and flowstone attached to the back wall of the cave. Cemented layers of sediment are common along the walls, where breccia of éboulis clasts and mud are indurated by carbonate cement. One notable exception is level GG, an extremely hard bed of large éboulis clasts and mud cemented by sparry calcite, which extends across the center of the main chamber. This level has a gentle dip of about 2–3° to the east and a variable thickness of approximately 15–40 cm where it is exposed in the deeper parts of the excavation. Levels HH-II represent the irregular lower parts of the hardpan, with HH an uncemented lens of muddy éboulis in between the firmly cemented levels GG and II (Table 2). Toward the cave opening (rows G and H), the cemented layer thickens and continues intermittently above GG into level BB.

The concentration of faunal remains and human artifacts in the sedimentary fill is quite variable between levels and also between locations in the cave (Table 2). Bone preservation is good throughout the cave sequence but bones are most abundant in the rear of the cave. The faunal assemblage is described in detail elsewhere (Bicho et al., 2006; Haws, 2012; Hockett, 1999; Hockett & Bicho, 2000; Hockett & Haws, 2002, 2009). The large bones mostly include mammals, such as red deer, ibex, horse, wild boar, and lynx, whereas the small bones are dominantly rabbits, birds, micromammals and amphibians. Levels T through X contain a superabundance of small animal bones in dense clusters that are likely associated with lynx or raptor predation. Most evidence of Paleolithic human occupation is also concentrated toward the rear of the cave. A series of prominent Magdalenian hearths, the largest of which was more than 2.5 m diameter and 40 cm thick (Bicho et al., 2006), dominate the sediments in Zone 1 that are rich in charcoal, ash, and crushed bone fragments. The large prepared hearth and associated features are the only areas where human activity appears to have significantly disturbed the sedimentary sequence. Human activity is otherwise limited to thin ephemeral hearths, typically represented by a few pieces of charcoal scattered amongst the éboulis clasts, and sporadic concentrations of artifacts, sometimes in association with modified animal remains. These modest human occupations appear to have alternated with periods of faunal occupation throughout the Pleistocene, with a trend toward more intensive human presence at the end of the Upper Paleolithic.

TABLE 2 Properties of stratigraphic zones and excavation levels as described in reference profile 1. Sampled locations are shown in Figures 4 and 5

Zone	Level	Depth interval (mbd)	Matrix color (Munsell)	Sediment description [a, b, c]	Lithic assemblage[d]
1	D	0.87–1.12	Brown (10YR5/3)	Medium clasts in very muddy matrix, friable to slightly hard, common fine charcoal and bone fragments, chalky appearance	Epipaleolithic
	E	1.12–1.86	Grayish brown(10YR5/2)	Small to medium clasts in very muddy matrix, friable to slightly hard, abundant charcoal and bone fragments, chalky appearance	Late Magdalenian
	F	1.86–2.17	Dark grayish brown (10YR4/2)	Medium to large clasts with little fine sediment, loose, muddy dark brown lenses with abundant charcoal and bone fragments	Late Magdalenian
	I	2.17–2.37	Light yellowish brown (10YR6/4)	Large to very large clasts with very little fine sediment, loose to friable, few bones	Late Magdalenian
	J	2.37–2.55	Yellowish brown (10YR5/4)	Medium to large clasts with very little fine sediment, loose, few bones	Late Magdalenian
2	K	2.55–2.75	Strong brown (7.5YR5/6)	Small clasts, friable, few bones	Early Magdalenian
	L	2.75–3.13	Strong brown (7.5YR5/6)	Small to medium clasts in muddy matrix, friable to slightly hard, few bones and fragments, few boulders up to 100 cm	Early Magdalenian
	M	3.13–3.19	Strong brown (7.5YR5/6)	Very small clasts in muddy matrix, friable	None
	N	3.19–3.53	Strong brown (7.5YR4/6)	Medium to large clasts, loose to friable, common medium-large bones and bone fragments	None
	O	3.53–3.81	Strong brown (7.5YR4/6)	Medium clasts, friable, common charcoal, and bones	Solutrean
	P	3.81–3.93	Brown (7.5YR4/4)	Medium to large clasts, loose to friable	None
	R	3.93–4.01	Brown (7.5YR5/4)	Small to medium clasts, friable, common charcoal, and small bones	Solutrean
	S	4.01–4.13	Light brown (7.5YR6/4)	Small clasts, friable, common charcoal, and bones	Solutrean
	T	4.13–4.86	Strong brown (7.5YR4/6)	Medium to large clasts, friable, common boulders up to 80 cm, muddy in lower half with abundant charcoal and bones	Solutrean and Proto-Solutrean
3	U	4.86–5.02	Strong brown (7.5YR5/6)	Small to medium clasts in muddy matrix, friable, includes lenses with abundant small animal bones and bone fragments	Terminal Gravettian
	V	5.02–5.12	Strong brown (7.5YR5/6)	Medium to large clasts, little fine sediment, loose to friable, abundant small animal bones	Gravettian
	W	5.12–5.25	Strong brown (7.5YR4/6)	Small to medium clasts in very muddy matrix, friable to slightly hard, abundant small animal bones and bone fragments	Gravettian
	X	5.25–5.32	Strong brown (7.5YR5/6)	Medium clasts, little fine sediment, friable, abundant small animal bones	Gravettian
	Y	5.32–5.53	Strong brown (7.5YR5/6)	Medium to large clasts, little fine sediment, common bones	None
	Z	5.53–5.71	Strong brown (7.5YR5/6)	Medium clasts in muddy matrix, friable, common bones	None
	BB	5.71–5.96	Strong brown (7.5YR5/6)	Large clasts, friable, common bones, few boulders up to 60 cm	Early Upper Paleolithic
	CC	5.96–6.03	Strong brown (7.5YR5/6)	Very small clasts, friable	None
	DD	6.03–6.14	Strong brown (7.5YR4/6)	Medium clasts in very muddy matrix, slightly to moderately hard	Early Upper Paleolithic
	EE	6.14–6.27	Reddish brown (5YR4/4)	Small clasts in muddy matrix, friable to slightly hard, common bones	None

(Continues)

TABLE 2 (Continued)

Zone	Level	Depth interval (mbd)	Matrix color (Munsell)	Sediment description [a, b, c]	Lithic assemblage[d]
	FF	6.27–6.45	Dark reddish brown (5YR3/4)	Medium clasts, slightly to moderately hard, abundant charcoal and bones	Early Upper and/or Middle Paleolithic
4	GG	6.45–6.62	Strong brown (7.5YR5/6)	Large clasts, extremely hard, cemented by calcite crystals filling voids, common bones, and bone fragments	Aurignacian
	HH	6.62–6.76	Strong brown (7.5YR4/6)	Medium clasts in muddy matrix, slightly hard, common bones	Aurignacian
	II	6.76–6.87	Strong brown (7.5YR5/6)	Medium to large clasts in muddy matrix, very hard, calcite cement filling voids	Aurignacian
	JJ (upper)	6.87–7.73	Reddish brown (5YR4/4)	Medium to large clasts in muddy matrix, slightly hard, common bones; up to 20 cm thick lenses of dark reddish brown fine sediment with dispersed charcoal	Mousterian
5	JJ (lower)	7.73–8.35	Reddish brown (5YR4/4)	Medium clasts in very muddy matrix, slightly hard, lenses of dark reddish-brown fine sediment with dispersed charcoal and large animal bones	Mousterian
	KK	8.35–8.64	Yellowish red (5YR5/8)	Medium to large clasts, slightly to moderately hard, few bones	None [e]
	LL	8.64–9.15	Reddish brown (5YR4/4)	Large clasts, slightly hard, concentration of angular boulders up to 60 cm in lower part	None [e]
	MM	9.15–9.98	Reddish brown (5YR5/4)	Medium to large clasts in muddy matrix, moderately hard, few small animal bones	None [e]
	NN	9.98–10.62	Reddish brown (5YR5/4)	Very large clasts and boulders up to 70 cm in muddy matrix, slightly hard, few bones	None[e]

[a]Clast size descriptors (modal class of long axis): very small, less than 15 mm; small, 15–30 mm; medium, 30–50 mm; large, 50–75 mm; very large, greater than 75 mm.
[b]Fine sediment content descriptors (sediment <2 mm, % by volume): very little fine sediment, less than 3%; little fine sediment, less than 10%; muddy matrix, 20–30%; very muddy matrix = 30–40%.
[c]Hardness descriptors: L: loose, no resistance to excavation; FR: friable, little resistance to excavation by trowel; SH: slightly hard, moderate resistance to excavation by trowel, MH: moderately hard, moderate resistance to excavation by hand pick, VH: very hard, strong resistance to excavation by hand pick; EH: extremely hard, large pick, chisel or sledge required to excavate.
[d]Cultural attribution given for levels with diagnostic artifacts (except Z, BB, DD which contain lithics of uncertain affiliation).
[e]Only 2 m^2 have been excavated to levels KK-NN; no artifacts have yet been recovered from these levels.

4.2 | Radiocarbon chronology

The 56 radiocarbon ages presented in Table 1 provide evidence for steady aggradation of the sedimentary surface in the cave between 9 and 45 ka. The samples show, generally, good age agreement within each level, and the levels maintain stratigraphic position with respect to age. A composite age-depth model was constructed from these ages to estimate sedimentation rates through time and to extrapolate approximate ages for undated deeper levels (Figure 7). Before modeling, seven of the 56 ages were rejected as being clearly too young for their depth below datum. We assume that these samples were contaminated by younger carbon infiltrating through large interstitial spaces from overlying horizons, as proposed by Bicho et al. (2006). After excluding outliers, a LOWESS smoothing technique was used to fit sample ages (±2σ cal age midpoint) to sample depths. The smoothing function employs weighted linear regression to assign an age to each 1 cm depth interval, based on a smoothing parameter of 0.25 and a tri-cubic weighting function. The result is a realistic age-depth model with residual errors typically less than ±1,000 years (RMSE, 926 years). In contrast, all of the ages that were rejected as outliers fall at least 7,500 years below the trend line. The relatively small nonoutlier errors are mainly due to the composite nature of the data set, where samples of similar age may lie at different depths due to the topography of the bedding. Thus the deposition model in Figure 7 represents spatially-averaged and smoothed aggradation for the cave sequence as a whole, although it is particularly tuned to the main excavation area where most samples were collected.

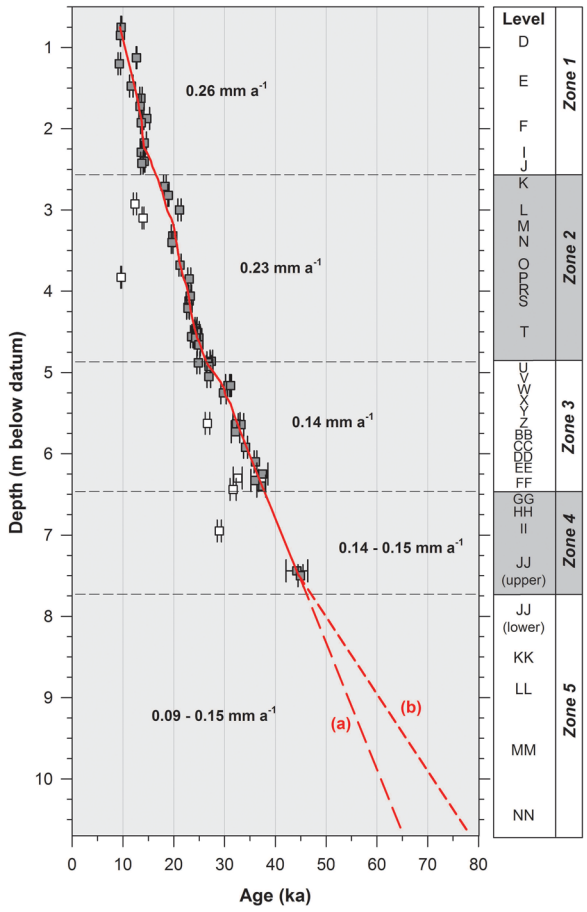

FIGURE 7 Composite deposition model based on radiocarbon ages shown in Table 1. Squares are plotted at the measured depth below datum (or midpoint of depth range) on Y axis, and at the midpoint of the ± 2σ calibrated age range (represented by whiskers) on X axis. White squares represent outlier ages not used in the deposition model. For stratigraphic context, boxes to the right show the sequence of stratigraphic levels and zones identified at reference profile 1. Two scenarios (a) and (b), discussed in the text, are shown for extrapolation of the deposition model to undated levels below Zone 4 [Color figure can be viewed at wileyonlinelibrary.com]

Based on the deposition model, average sedimentation rates show a near doubling for zones 1 and 2 (0.23–0.27 mm a^{-1}) compared with zones 3 and 4 (0.14–0.15 mm a^{-1}; Figure 7). Shorter-term sedimentation rates calculated over 2,000-year intervals vary between 0.09–0.33 mm a^{-1}. The sedimentation rate increases toward the top of the section, with accelerations occurring near the base of both zones 1 and 2. By contrast, the sedimentation rate appears to be fairly steady throughout zones 3 and 4 at the bottom of the radiocarbon-dated sequence.

Linear extrapolation below the radiocarbon-dated levels, extending the sedimentation rate that prevails in zones 3 and 4 to the base of the excavation, yields an estimated age of 65.0 ka at a depth of 10.62 mbd (Figure 7, Scenario a). An alternate model for Zone 5, based on extrapolation and tuning to the NGRIP ice core record, suggests an older basal age of 77.8 ka (Figure 7, Scenario b). These scenarios are discussed in more detail below.

4.3 | Sediment texture

Éboulis clasts in the coarse pebble (20–75 mm), cobble (75–200 mm), and boulder (>200 mm) size ranges make up a majority (60–98% by volume) of every stratigraphic level encountered in the cave. Mean large clast measurements at the reference profiles (Figure 8) show periodic depth fluctuations, consistent with the modal clast size categories determined during excavation (Table 2). Both reference profiles show a slight and irregular increase in large clast size with depth. Large boulders are found sporadically throughout the main excavation area but are especially common in levels L, T, BB, LL, and NN (Table 2). Boulder concentrations in levels L and T reflect large-scale roof failure near the cave entrance, with blocks sliding down the éboulis ramp into the cave interior. The small portions of levels LL and NN examined to date contain large, angular blocks with random orientations, perhaps reflecting major roof collapse events within the main chamber.

The fine sediment fraction (<2 mm), after removal of organic matter, is dominated by silt, which typically comprises 70–80% of the fine fraction (Figure 8). Almost all samples have modal and median particle size in the fine to medium silt range (10–25 μm), poor to very poor sorting (3.5–6.0 μm), and slight negative skewness (0 to − 0.3). Depth trends are subtle but include increasing clay and decreasing sand content with depth. Sand, almost entirely fine and very fine,

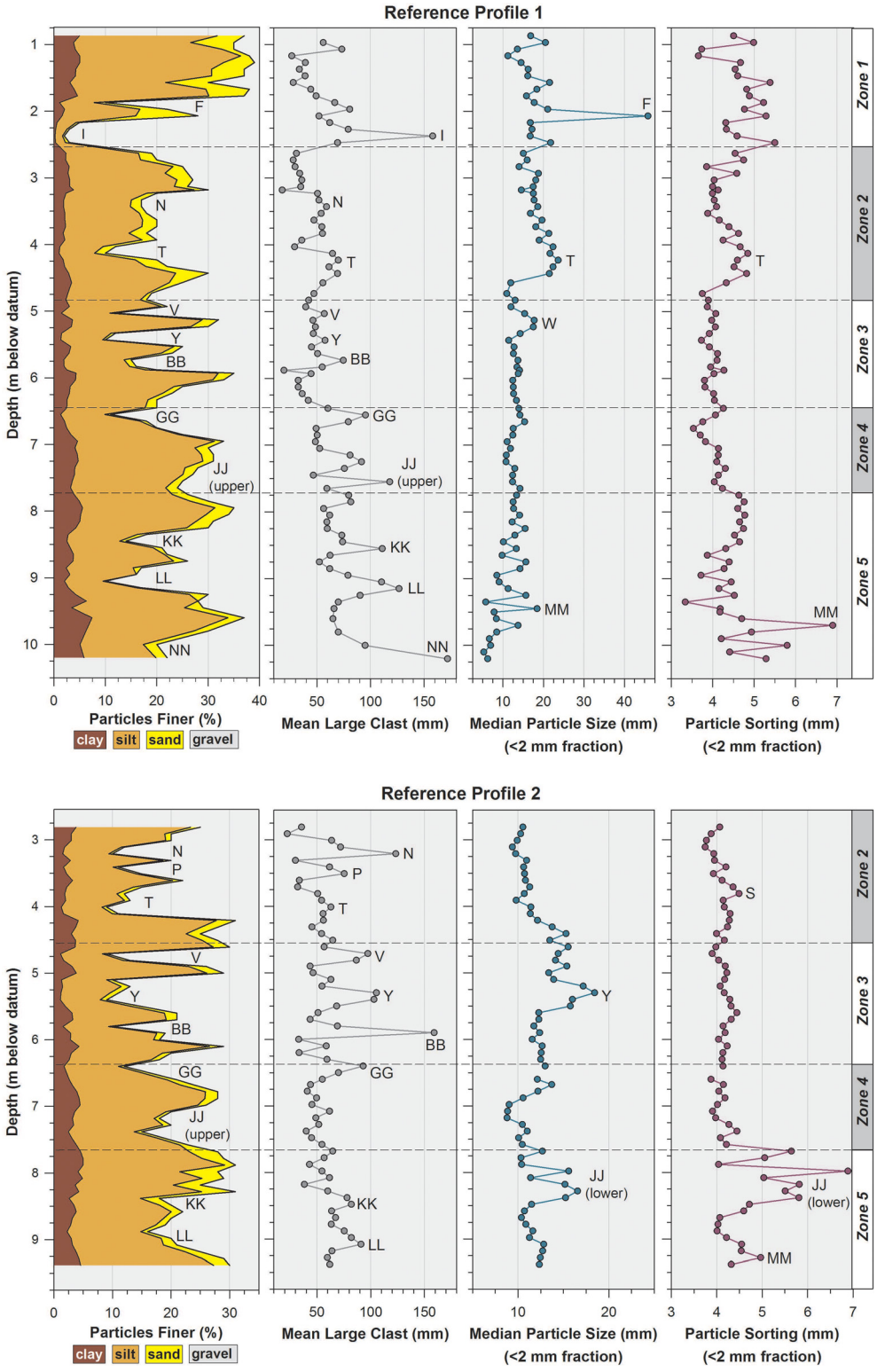

FIGURE 8 Particle size data for the two reference profiles. Size separates are based on field estimates of % gravel combined with laser diffraction analysis on the fine-grained fraction (<2 mm). Mean large clast size is a measure of the Five largest clasts visible in each 10 cm depth interval of a 1 m wide section of the profile wall. Sampling locations are shown in Figures 4 and 5. Notable features of each plot are labeled with corresponding levels (described in Table 2) [Color figure can be viewed at wileyonlinelibrary.com]

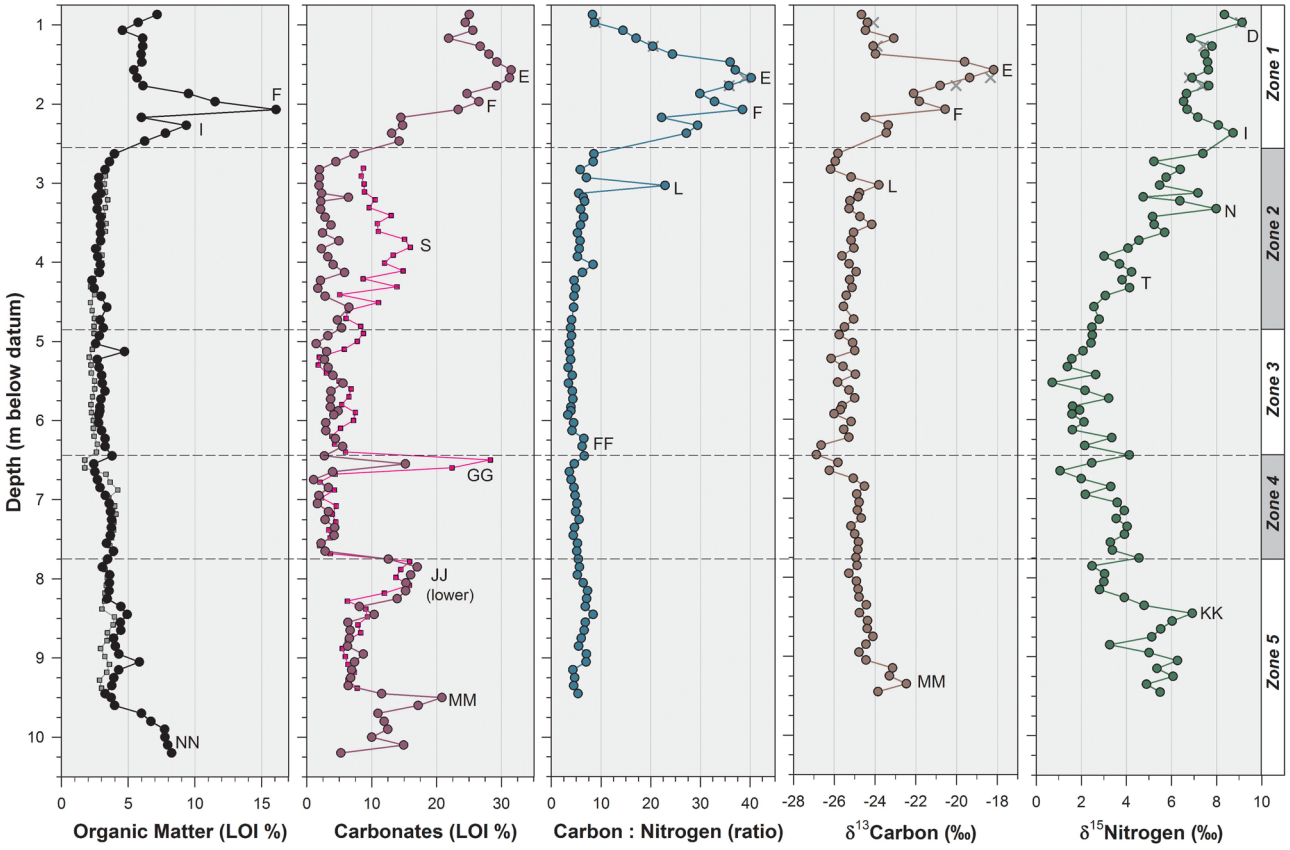

FIGURE 9 Composition data for the two reference profiles. Loss on ignition data (organic matter and carbonates) are given for both reference profile 1 (black circles) and 2 (gray squares). Carbon/nitrogen ratio and isotope data are for reference profile 1 only. Gray Xs are replicate samples that were analyzed to demonstrate data reliability. Sampling locations are shown in Figures 4 and 5. Notable features are labeled with corresponding levels (Table 2) [Color figure can be viewed at wileyonlinelibrary.com]

generally comprises <15% of the fine fraction, except in Zone 1 where it is as high as 30%.

4.4 | Fine sediment composition: Loss on ignition

Carbonates comprise up to one-third, and organic matter up to one-sixth, of the fine sediment fraction by weight. At reference profile 1, the largest concentration of carbonates and nearly all of the organic matter occur in Zone 1 (Figure 9). Profile 2 is broadly similar but contains additional carbonates at 3–4 mbd due to its location near the cave wall. Both profiles show 15–30% carbonate in the cemented level GG, and another zone of elevated carbonates in the lower part of level JJ. The presence or absence of carbonates is the most obvious feature of the fine sediment fraction in the laboratory data and is a major factor in differentiating the five stratigraphic facies.

The levels with elevated carbonate (E-F, GG, JJ, MM) appear to belong to several different types. Levels E and F are associated with Magdalenian hearths and probably include a large contribution of pyrogenic calcite from wood ash. These levels are friable to moderately hard, have a chalky/crumbly consistency, and contain abundant charcoal, lithics, and crushed bones (Table 2). Layer GG, by contrast, is an extremely hard layer with few bones, no charcoal, and sparry calcite cementing the large éboulis lasts. Layer GG forms an extremely hard, gently dipping platform across the center of the cave at the top of stratigraphic Zone 4, which is otherwise broadly similar to Zone 3. The other carbonate-rich levels (lower JJ, MM) exhibit slight to moderate hardness but have no visible accumulation of secondary carbonates. The source of carbonates in these beds is unclear, as presently only a few m^2 have been exposed in the deepest part of the excavation.

Another carbonate and organic matter rich cemented layer (not represented in reference profiles 1 or 2) marks the top of the sedimentary sequence in the niche area. This hardpan, assigned to level F, is laterally contiguous with the Magdalenian hearth that marks the organic matter peak in reference profile 1. After sediment filled the opening that connects the niche with the main chamber, flowstone covered the walls of the small room effectively sealing it shut. Radiocarbon ages on charcoal and bone from the surface of the niche area (units ZZ9-ZZ10) date to the Late Magdalenian, 13.5–14.3 cal ka BP (Table 1). Thus the filling and closure of the niche area occurred during the same time period that the large Magdalenian hearth was built in the main excavation area.

The combustible organic matter peak in Level F represents the intersection of reference profile 1 with the large Magdalenian hearth investigated by Bicho et al. (2006). Charcoal and faunal

remains are the main organic components recognized during excavation. Localized pockets of higher organic matter were identified in other parts of the cave, such as in the niche area where charcoal and bone concentrations occur in a series of small stacked hearths (15–25% OM in hearth sediment from levels O, R, and T). All samples from inside the cave with >6% organic matter are associated with anthropogenic combustion features that were easily identified during excavation.

4.5 | Fine sediment composition: Organic carbon and nitrogen

The composition of the organic fine sediment fraction is inferred from field evidence along with stable carbon and nitrogen isotopes, and carbon/nitrogen ratios, which are commonly used as indicators of organic matter types and sources, such as terrestrial versus marine organic compounds, vegetation communities, such as grassland versus forest, or trophic position in food webs (Finlay & Kendall, 2007; O'Leary, 1981; Peterson & Fry, 1987). Although bulk organic carbon and nitrogen isotopes from soils and sediments contain some information on organic matter cycling, a compound-specific isotope approach would better resolve spatial and temporal patterns associated with particular biomarkers (Bi, Sheng, Liu, Li, & Fu, 2005; Collister, Rieley, Stern, Eglinton, & Fry, 1994; Diefendorf & Freimuth, 2017; Gleixner, 2013; Taylor, Benedetti, Haws, & Lane, 2017). Here we are limited to bulk analysis of organic $\delta^{13}C$ and $\delta^{15}N$ isotope ratios from fine sediment samples collected at reference profiles 1 and 2. These samples integrate organic matter from multiple sources, which likely include soil organic matter from outside the cave, charcoal and other plant matter introduced to the cave, animal remains including crushed bone and shell fragments derived from faunal or anthropogenic activities and microbial or algal activity within the cave environment. Although this analysis is rather coarse-grained, some inferences can be drawn based on typical $\delta^{13}C$ values derived from the ecological literature: soil organic matter under C_3 plant communities averages about − 25‰ to − 30‰ (Finlay & Kendall, 2007; Peterson & Fry, 1987), charcoal and wood ash − 23‰ to − 26‰ (Shahack-Gross et al., 2008), bone and tooth collagen of terrestrial herbivores and carnivores − 19‰ to − 24‰ (Bocherens et al., 1997; Peterson & Fry, 1987). Values of $\delta^{15}N$ for soils average +2‰ to +5‰ (Finlay & Kendall, 2007), whereas animal bones and tissues demonstrate ^{15}N enrichment 3–5‰ higher than their dietary sources (Peterson & Fry, 1987). Microorganisms tend toward a narrow range of C:N ratios between 5 and 12 (Gleixner, 2013) and cause a variety of C and N fractionation effects, but microbial decomposition in soils and sediments favors a modest enrichment in both $\delta^{13}C$ and $\delta^{15}N$ ratios (Finlay & Kendall, 2007; Peterson & Fry, 1987).

Reference profile data from Picareiro show that low C:N ratios (≈ 5), strongly negative $\delta^{13}C$ ratios (− 24 to − 27‰), and moderate $\delta^{15}N$ ratios (+4 to +8) prevail for the entire sedimentary sequence below level L (Figure 9). We interpret these values as indicating a fairly uniform source of organic matter over time, mainly derived from soils outside the cave and modified by microbial activity inside the cave. The carbon isotope values are consistent with those cited above from the ecological literature as typical values for C_3 vegetation, along with previous cave studies in C_3 regions, such as Forbes, Bestland, Wells, and Krull (2007). The cave sediments exhibit $\delta^{13}C$ ratios that are slightly higher than the average of − 27‰ reported by Finlay and Kendall (2007) for soil organic matter, which could reflect fractionation by microorganisms. A significant microbial component would also favor the low C:N ratios exhibited throughout most of the Picareiro sequence. Some levels with elevated $\delta^{15}N$ values (+4 to +8‰) occur in Zones 2 and 5, despite persistent low values of organic matter content, C:N ratio, and $\delta^{13}C$ Figure 9). Similarly enriched $\delta^{15}N$ in the absence of enriched $\delta^{13}C$ have been cited in other cave environments and may be ascribed to accumulations of animal feces or guano, or in some cases to the activity of algae or chemoautotrophic bacteria (Engel, 2005; Forbes et al., 2007; Pohlman, Iliffe, & Cifuentes, 1997; Sarbu, Kane, & Kinkle, 1996). Taken together, the carbon and nitrogen data from below Zone 1 are consistent with a cave ecosystem that has limited sources of organic carbon, and thus low primary productivity.

In sharp contrast, Zone 1 stands out with substantially higher $\delta^{13}C$ ratios (− 24‰ to − 18‰), $\delta^{15}N$ ratios (+7‰ to +9‰), and C:N ratios 10–40) than the rest of the sedimentary sequence (Figure 9). This pattern is likely due to the abundance of small bone fragments and other organic matter derived from animal remains in the Magdalenian hearths that were excavated in levels E, F, and J (Table 2). Examination of samples from levels E-F under a hand lens shows a significant amount of crushed and burned bone in the fine sediment fraction, along with shell, charcoal, wood ash, limestone fragments, and some quartz sand. This is consistent with observations of Bicho et al. (2013) who concluded that the hearths were used to crush bones and extract marrow. Organic matter in these levels undoubtedly comes from a variety of sources, but their carbon and nitrogen isotope ratios fall within the range reported for bone and tooth collagen by Bocherens et al. (1997), and the $\delta^{13}C$ values are broadly similar to those obtained on bones analyzed for radiocarbon dating in this study (Table 1). Because C_4 plants comprise a very small proportion of the vegetation in this region (Still, Berry, Collatz, & DeFries, 2003), and inorganic carbonates were removed from the samples before analysis, faunal and anthropological inputs are the most likely explanation for the large $\delta^{13}C$ excursion in the upper part of the sequence at Picareiro. At this scale of bulk analysis, the stable isotope data do not contain any obvious correlation to fluctuations in paleoclimate, sedimentation rate, or sediment composition. Instead, with the exception of the Magdalenian hearth levels, these data demonstrate relative stability of organic matter forms and sources over a very long period. Biomarker studies are underway at the site that will further illuminate these topics in the future.

4.6 | Fine sediment composition: Elemental geochemistry and mineralogy

Fine sediments in the reference profiles are mainly aluminosilicates with varying degrees of calcite enrichment. From most to least

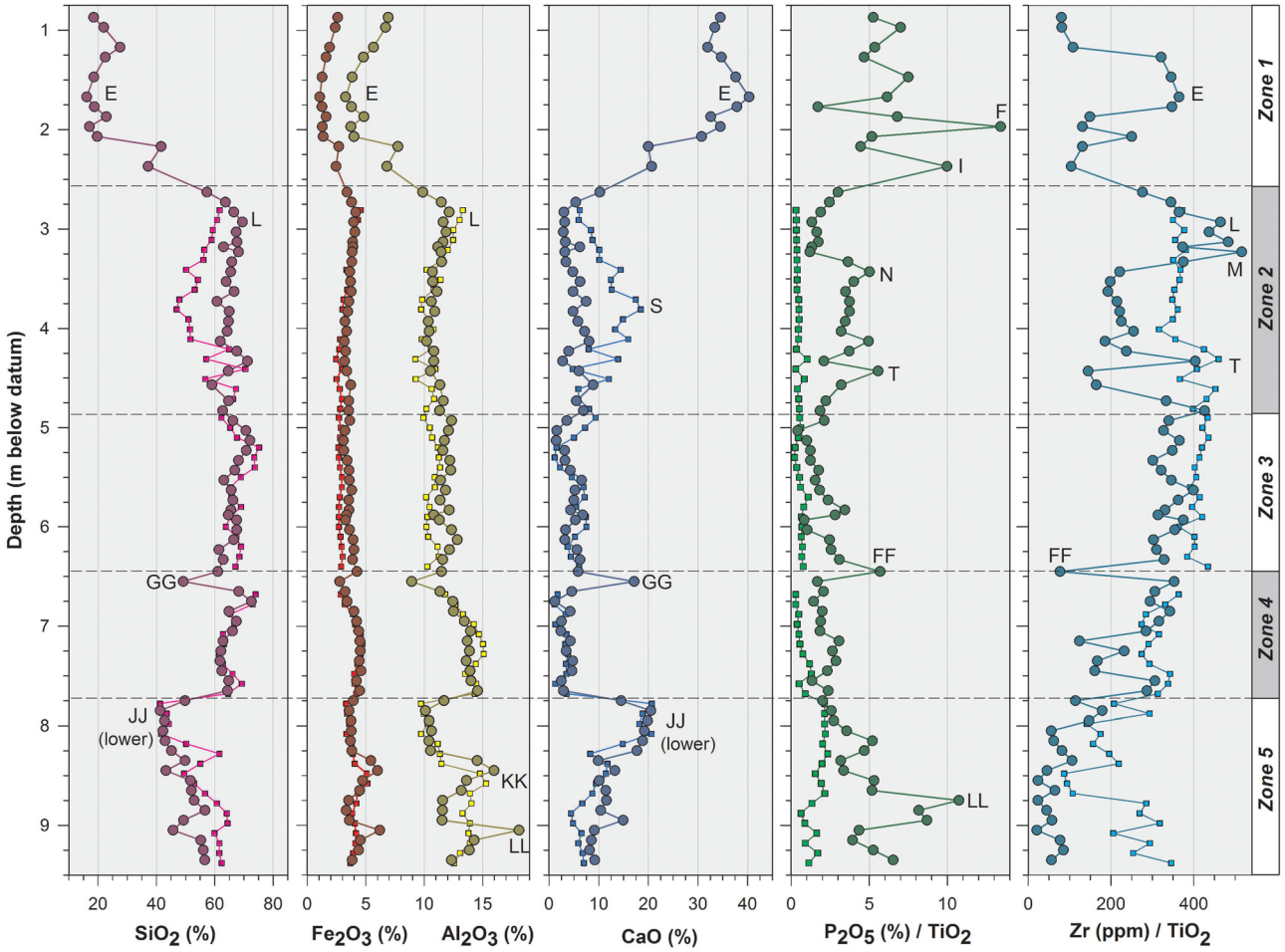

FIGURE 10 Concentration of major oxides and trace elements for reference profile 1 (black circles) and 2 (gray squares). Concentrations for rare elements are expressed relative to % TiO_2 to remove the dilution effect caused by carbonate enrichment in zone 1. Sampling locations are shown in Figures 4 and 5. Notable features are labeled with corresponding levels (Table 2) [Color figure can be viewed at wileyonlinelibrary.com]

abundant, the major oxides present are SiO_2 (depth-averaged abundance = 57.9%), Al_2O_3 (11.3%), CaO (9.6%), Fe_2O_3 (3.5%), K_2O (2.6%), P_2O_5 (1.4%), and TiO_2 (0.6%). Other oxides (MgO, Na_2O, MnO) amount to less than 1% in all samples. Depth variations show that Zone 1 is dominated by CaO and low SiO_2, in agreement with the high carbonate content determined by LOI. Zones 2–4 are dominated by SiO_2 with low CaO, and Zone 5 is intermediate between these (Figure 10). SiO_2 is positively correlated with most of the common metals and bases (Al, Fe, K, Mg, Na, Ti), whereas CaO is inversely correlated with SiO_2 and positively correlated with P, Mn, and Sr. Phosphate (P_2O_2/TiO_2) is elevated in bone-rich levels (F-J, N-T, FF), and also in level KK where bones are not abundant but where elevated $\delta^{15}N$ ratios suggest another source of organic matter such as guano. The trace element zirconium (Zr/TiO_2) attains a peak in levels L-M, some of which may be eolian in origin given the common Zr enrichment in eolian sediments (McLennan et al., 1993).

Aside from the variable degrees of calcite enrichment, the elemental content of the fine sediment fraction implies a uniform sediment source through time. The relative proportions of Si, Al, and Fe in these samples are typical of aluminosilicate clay minerals derived from limestone weathering and/or eolian deposition in other cave settings (e.g., Kim et al., 2013; Arriolabengoa et al., 2015). The clay minerals present are almost certainly kaolinite and illite considering their dominance in nearby soils and in similar karst settings in Portugal (Fonseca, Barriga, & Conceição, 2010; Lourenço, Rocha, & Gomes, 2012; Rocha & Gomes, 1996). Field observations with a hand lens show that the sand and coarse silt fractions are composed of mostly quartz and limestone fragments, with trace amounts of heavy minerals.

4.7 | Magnetic susceptibility

MS data published by Ellwood et al. (2001) established a baseline for interpreting paleoclimate phases from sedimentary sequences in caves across Mediterranean Europe, including the uppermost part of the sequence at Lapa do Picareiro. They argued that the MS signal of detrital sediments in caves reflects subaerial weathering processes outside the cave that form and concentrate magnetic minerals. These minerals are then transported in sediments to the cave by eolian processes, surface runoff, or infiltration through karst conduits. Quaternary cave sequences can produce fairly robust paleoclimate proxies from MS records because mineralogical impacts on surface

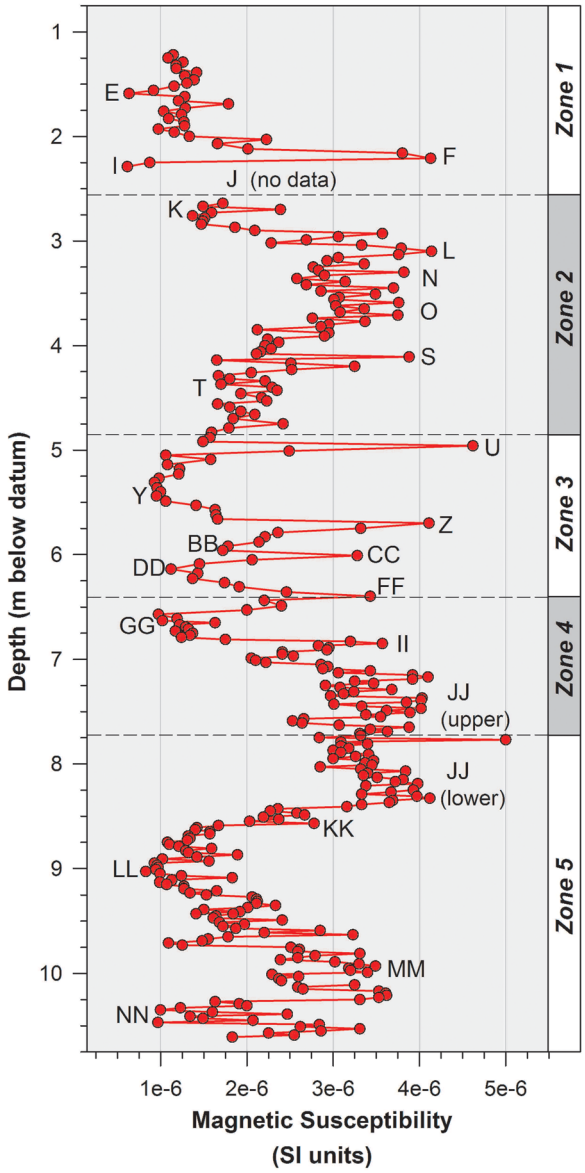

FIGURE 11 Magnetic susceptibility for fine sediment samples collected adjacent to reference profile 1. Data from 1.2 to 2.3 mbd were published previously by Ellwood et al. (2001) before establishing the current cave datum. Level J (2.35–2.60 mbd) is not represented due to insufficient fine sediment to collect an MS sample. Sampling locations are shown in Figures 4 and 5. Notable features are labeled with corresponding levels (Table 2) [Color figure can be viewed at wileyonlinelibrary.com]

sediments due to climate change are large and occur rapidly, and because protected cave settings lead to minimal diagenetic alteration (Ellwood et al., 1998; 2001; 2004).

The complete MS data set from Lapa do Picareiro is presented in Figure 11, including previously published data for samples above 2.5 mbd. MS values fluctuate rapidly between $1–5 \times 10^{-6}$ m^3 kg^{-1}, comparable to values from nearby Oliveira and Caldeirão caves in Portugal but an order of magnitude greater than values reported for other caves in Spain and Albania (Ellwood et al., 2001). The magnetic signal at Picareiro is likely produced by hematite and fine-grained goethite and maghemite, which were the primary magnetic minerals reported for Caldeirão Cave from XRD and Mössbauer spectroscopy (Ellwood et al., 1998). No significant correlation was detected between MS and any of the particle size or composition parameters, demonstrating that the MS signal is mainly determined by mineralogical variations and not simply by enrichment in sand or secondary carbonates.

Several sharp peaks appear in the MS record (within levels F, L, S, U, Z, CC, FF, II, JJ, MM), along with some strong negative excursions (levels E, I, T, Y, DD, GG, LL, NN). The high frequency and large magnitude of fluctuations support the notion of Pleistocene paleoclimate as a primary control on MS in the cave sequence, as discussed below. Several of the MS peaks correspond with organic-enriched levels (F, FF, JJ). This is especially true for the Magdalenian hearth in level F. It is possible that the MS peak in Level F is partly an artifact of the hearth, given that MS has been shown to be enhanced by burning in some settings (Herries, 2006; Woodward & Bailey, 2000), although not universally (Woodward et al., 2001). For the Magdalenian deposits at Picareiro, the organic matter peak of the hearth structure (Figures 9) is much thicker than the MS peak (Figure 11). Also, the MS peak in Level F is no greater than other MS peaks that are not associated with hearths or charcoal concentrations. Thus combustion features do not appear to have strongly influenced the MS signal.

4.8 | Targeted soil, rock, and speleothem samples

A small number of targeted samples were analyzed to compare various components of the cave sedimentary system: (a) surface soils outside and above the cave ($n = 7$), (b) limestone clasts from the sedimentary fill within and immediately outside the cave ($n = 5$), (c) muddy sediment recovered from narrow joints and crevices in the cave walls ($n = 3$), and (d) secondary carbonates in the form of large calcite crystals and the cemented matrix of breccias in the sedimentary fill ($n = 3$). Radiocarbon analyses of bone and charcoal samples also produced ^{13}C data (Table 1) that are included here for comparison. Select compositional and geochemical properties of these samples are compared with fine sediment samples from zones 1, 3, and 5 of the reference profiles in Figure 12.

Surface soils contain concentrations of common oxides that compare favorably with those from the reference profile samples inside the cave. Samples from the lower excavation levels (zones 2–5) especially match the surface soils for the building blocks of aluminosilicate minerals, such as Si, Al, Fe, Mn, Mg, K, and Na. In contrast, concentrations of CaO are low in surface soils and high in limestone clasts. The high proportion of CaO (mean = 55%) and low proportion of MgO (mean = 0.5%) in the analyzed limestone clasts are consistent with description of the Serra de Aire Formation as high-purity limestone with at least 95% calcite content (Carvalho, 2018), which can contribute to both karst dissolution and precipitation of speleothems. Crevice fills and secondary carbonates exhibit moderately high CaO concentrations that are broadly similar to the Zone 1 samples from the reference

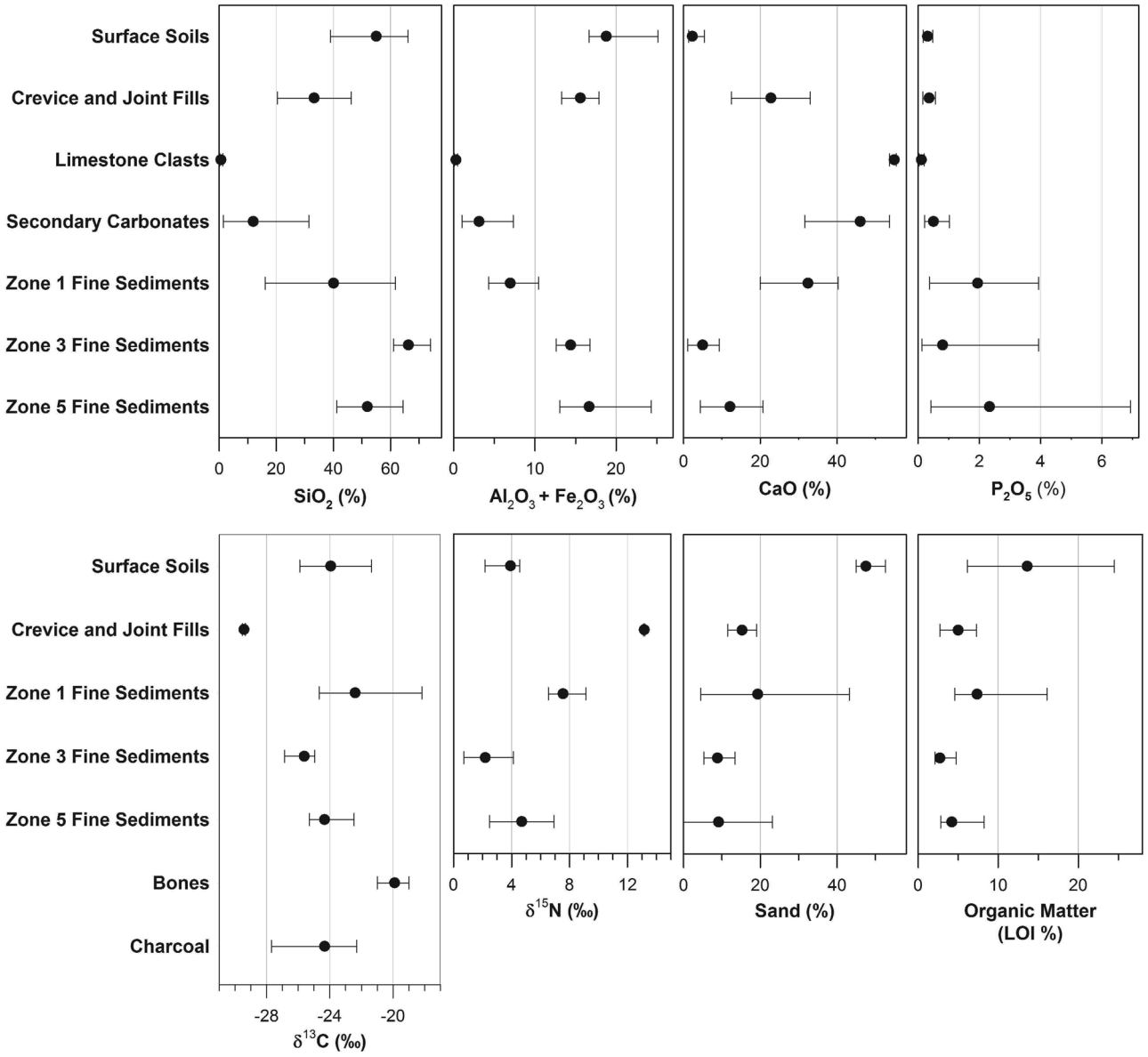

FIGURE 12 Comparison of select properties from samples of surface soils outside and above the cave, fine sediment collected from crevices and joints in the cave wall, limestone clasts collected from the cave fill, secondary carbonates including calcite crystals and flowstones, and reference profile samples from stratigraphic zones 1, 3, and 5. Carbon isotope ratios are shown for radiocarbon samples of bone and charcoal (Table 1). Dot and bar represent the mean and range for each sample

pits. The trace element Sr is also elevated in limestone clasts relative to cave sediments and surface soils. P_2O_5 stands out for having reference profile concentrations that fall well above those of the surface soils, limestone clasts, crevice fills, and secondary carbonates.

The particle size characteristics of crevice fill sediment closely resemble the <2 mm fraction of the reference profile samples, with roughly 10–20% sand, 10–15% clay, median size in the fine-medium silt range (10–20 μm), and poor to very poor sorting (Figure 12). By comparison, the surface soils are coarser with around 50% sand and median size in the very fine sand range (60–75 μm). Organic matter is much higher in the surface soils than in the reference profile samples, with up to 25% organic matter in surface A horizons (Figure 12). Only the large Magdalenian hearth in Level F (Zone 1) approaches this value inside the cave, with up to 16% organic matter. Organic matter in the crevice fills resembles the reference profile samples from zones 2–5. Stable carbon and nitrogen isotopes for the surface soils are broadly similar to the reference profile samples, with the exception of Zone 1 which appears to be enriched by animal remains as discussed above. The crevice fill sediments contain little organic matter but very strongly enriched $\delta^{15}N$ and strongly depleted $\delta^{13}C$. This pattern requires more sampling and analysis, but resembles the unusually high $\delta^{15}N$ in the absence of high $\delta^{13}C$ that was noted above for sediments in zones 2 and 5, and is perhaps related to the microbial activity.

5 | DISCUSSION

5.1 | Site formation processes

The sedimentary fill at Lapa do Picareiro has five main components: éboulis, boulders, fine sediment, secondary carbonates, and organic matter. Clastic sediments in the cave are dominated by limestone éboulis, mostly 20–200 mm that comprise between 60% and 100% of the sediments by volume. Limestone boulders up to several meters long are concentrated near the entrance to the cave. Void spaces between the limestone clasts are filled with muddy fine sediment, predominantly aluminosilicate minerals although some deposits contain as much as 10–30% carbonates. Organic matter is a locally-significant component of the cave fill, mostly restricted to charcoal-rich hearths, such as level F, and dense bone clusters, such as level T. Certain components that are commonly found in other cave sequences have not been encountered in Lapa do Picareiro, including exogenic fluvial deposits, thick guano deposits, or accumulations of collapsed or degraded speleothem fragments.

Previous sedimentological studies in shallow limestone karst suggest likely modes of deposition for these various components (Farrand, 2001; Weiner, 2010; White, 2007; Woodward & Goldberg, 2001; Morley & Woodward, 2011; Karkanas & Goldberg, 2016). The apparent intensity of these processes at Lapa do Picareiro is summarized in Table 3 and discussed below. Éboulis, which makes up the majority of the sedimentary fill at Picareiro, is primarily derived from mechanical weathering of the cave roof and walls. Larger clasts and boulders represent episodic roof collapse and retreat of the cave opening. Small-scale debris flows and rockslides are commonly recognized where sediment accumulates near a cave opening and gradually moves into the cave. In general, fine sediment may be introduced into caves by a variety of fluvial, eolian, or colluvial pathways, each of which would imply different sediment sources, lag times, and sedimentological properties. The dominant fine sediment deposition process at Picareiro appears to be infiltration of weathered soil through bedrock fractures and karst conduits, an important process that has been previously reported in limestone karst and terra rossa settings across the Mediterranean (Bar-Yosef, 1993; Farrand, 2001; Woodward, 1997; Woodward & Bailey, 2000). Secondary carbonates accumulate in caves mainly by precipitation of dissolved karst byproducts to form speleothems, or from biotic sources such as wood ash or guano. Finally, some caves (including Zone 1 of the sequence at Picareiro) contain significant amounts of organic matter contributed by animal remains, fecal enrichment, and anthropogenic features such as hearths or waste pits.

Several rock-weathering processes were likely active at Lapa do Picareiro during the Pleistocene, including frost weathering, jointing by pressure release, root wedging, clay hydration, and corrosion associated with vadose flow and condensation of water vapor. Although snow and frost were common in the Pleistocene climates of Iberia, the precise role of frost weathering at Picareiro is difficult to determine because clast size and shape parameters do not produce conclusive evidence of cryoclastism (Woodward & Goldberg, 2001). Congelifracts and cavernously corroded clasts—rocks altered by postdepositional weathering that have been used to infer paleotemperature (Skaberne et al., 2015; Turk & Turk, 2010)—are either rare or absent in the interior of Lapa do Picareiro. Similarly, frost slabs—clasts with a thickness less than one-quarter the maximum width in the scheme of Laville et al. (1980)—are rare in the sections analyzed. Nevertheless, the evidence for frost action is strong given the angularity and moderately well-sorted nature of the éboulis beds. Such sediments demonstrate "lithological evidence of cryoclastism" as defined by Mallol et al. (2012), and are consistent with other descriptions of éboulis production in caves across Southern and Western Europe (Farrand, 2001; Goldberg,

TABLE 3 Summary of depositional processes responsible for site formation at Lapa do Picareiro

Sediment fraction	Depositional process	Evidence	Apparent intensity
Coarse clastic (boulders, éboulis, lithics)	Roof collapse	Large blocks near cave entrance	Moderate
	Spalling	Éboulis-dominated sediment throughout cave	Strong
	Faunal input	Gastrolith pebbles in some fauna-rich beds	Minor
	Human input	Lithic artifacts in occupation levels	Minor
Fine clastic (sand, silt, clay)	Infiltration	Poorly sorted matrix filling spaces between clasts	Strong
	Debris flows	Floating/imbricated clasts in poorly sorted matrix	Moderate
	In situ weathering	Corroded clasts, small limestone fragments	Minor or none
	Eolian	Lack of well-sorted, finely-stratified fine sediments	None
	Fluviokarst	Lack of sorted, stratified, or rounded sediments	None
	Faunal/human	Elevated sand content in zone 1 (?)	Minor
Chemical precipitates (carbonates, phosphates)	Karst precipitation	Speleothems on cave walls; Level GG flowstone	Minor to moderate
	Reworked ash/bone	Elevated carbonates with charcoal/bone in hearths	Minor to moderate
	Reworked guano	Elevated phosphate below Level JJ (?)	Minor or none
Organic (detrital)	Anthropogenic input	Charcoal, bone, shell in hearths	Minor to strong
	Faunal remains	Bone-rich predator occupation levels	Minor to strong
	Burrowing/nesting	Krotovina near cave entrance and along walls	Minor
	Fecal inputs	^{15}N enrichment in organic matter	Moderate

Laville, & Meignen, 2007; Laville et al., 1980; Woodward & Bailey, 2000). The semiperiodic nature of clast size fluctuations throughout the excavated area also supports a climatic control on éboulis production, with frost action the most likely cause. Boulder concentrations in a few levels appear to be associated with roof collapse near the cave mouth. Earthquakes are a possible contributor to this process given the historical seismicity in the region (Chester, 2001).

Several lines of evidence suggest that the fine sediment fraction at Picareiro is derived mostly from weathered terra rossa soil transported by infiltration through joints and crevices. In some cases, this sediment may have been remobilized by small-scale debris flows after accumulating near the cave entrance. Fine sediments in the cave are unstratified and poorly sorted and are broadly similar to surface soils and crevice fills in terms of color, texture, and geochemistry (Figure 12). Particle size distributions imply that much of the fine sediment could be derived from flow through crevices and joints that restrict transport of medium and coarse sand (>200 μm), which is abundant in surface soils but uncommon in the cave. It, therefore, appears that the bulk of the fine sediment fill at Lapa do Picareiro is derived from proximal sources, for example, the bedrock and terra rossa soils surrounding the cave. Some of the Zone 1 sediments contain appreciable medium and coarse sand, requiring an additional source of sand that might include slope wash or human and faunal inputs. No well-sorted or stratified fine sediment (eolian, fluvial) beds have been encountered in the cave to date. Given the role of eolian enrichment in terra rossa soil formation (Muhs et al., 2010), it is likely that some eolian deposits have been introduced to the cave, either by minor direct deposition through the cave opening or indirectly by infiltration through bedrock crevices.

Breccias cemented by calcite make up a small but significant proportion of the sedimentary fill at Picareiro. The cemented beds identified in the cave include those that are indurated by both geogenic calcite (precipitated from vadose waters) and pyrogenic calcite (derived from wood ash). Strong carbonate enrichment in Zone 1 forms the most obvious stratigraphic division in the entire cave sequence, distinguishing all the sediments above Level J from all the sediments below. Abundant bone and charcoal fragments associated with hearths support pyrogenic ash as the major source of calcite in Zone 1. Outside of Zone 1, clearly geogenic breccias are present that contain very little organic matter, including the hardpan of level GG which is cemented by sparry calcite crystals, and minor flowstone deposits along the cave walls. The uncemented but carbonate-rich sediments of Zone 5 are currently unexplained, but pyrogenic, geogenic, and biogenic calcite are all possible contributors. Future analysis including microarchaeological approaches will provide further insight on components of the fine sediment fraction, as suggested by previous findings by such methods at many cave and rock shelter sites (Bailey & Woodward, 1997; Courty & Vallverdu, 2001; Macphail & Goldberg, 2000; Woodward et al., 2001; Kourampas et al., 2009; Karkanas & Goldberg, 2010; Mallol et al., 2010; Weiner, 2010; Morley & Woodward, 2011).

5.2 | Sedimentation rates and chronology

The radiocarbon data and composite deposition model (Table 1, Figure 7) show fairly continuous sedimentation between 9 and 45 ka at rates between 0.1–0.3 mm a^{-1} (roughly 3–10 ka m^{-1}), which are typical for caves in Mediterranean Europe (Farrand, 2001). The average sedimentation rate clearly increased after about 25 ka, with a near doubling between zones 3–4 (0.14–0.15 mm a^{-1}) and zones 1–2 (0.24–0.26 mm a^{-1}). This increase in sedimentation rate was roughly coincident with HS2, but accelerated rates continued through the end of the Pleistocene. Accelerated sedimentation after 25 ka could reflect enlargement of the cave mouth or enhanced flow through karst conduits. It could also have resulted from changes in the shape of the cave. Survey data show that the depositional surface area inside the cave decreased significantly after 25 ka, as sediment filled alcoves surrounding the large chamber and eventually began to impinge upon the sides of the dome-shaped roof. Some of the accelerated sedimentation after 25 ka may be accounted for by intensive human use of the cave during the Magdalenian, including accumulation of bone, ash, charcoal, and lithic artifacts in the hearths. Similarly, the accumulation of very dense bone concentrations associated with both predators and humans in Level T may have contributed to an accelerated pace of sedimentation overall.

Among the most important features of the sedimentary sequence at Lapa do Picareiro is nearly 2 m of sediment between levels X-JJ dating to the Middle-Upper Paleolithic transition period, which has been proposed by various authors to date between 45 and 30 ka in Iberia (Finlayson & Carrion, 2007; Galvan et al., 2014; Higham et al., 2014; Marin-Arroyo et al., 2018). At present, the latest confirmed Middle Paleolithic occupation is in level JJ, which has several thin horizons of Mousterian artifacts associated with charcoal and modified faunal remains dated to around 45–47 ka. The earliest Upper Paleolithic is a chert bladelet industry in levels GG-HH-II from the back of the cave that reveals a previously unknown Early Aurignacian presence in central Portugal (Haws et al., 2018). Several overlying levels also contain Early Upper Paleolithic artifacts, represented by chert flakes and blades (levels BB and DD) and quartz and quartzite flakes (level FF). Collectively, these Early Upper Paleolithic levels (BB–II) are associated with radiocarbon ages between 33.7–38.5 cal ka BP (Table 1), aligning well with the Early Aurignacian starting around the time of HS4 in southern France and northern Spain (Bataille, Tafelmaier, & Weniger, 2018; Mora et al., 2018; Straus, 2015; Wood et al., 2014). A separate artifact concentration of uncertain cultural affiliation in Level FF of the main excavation area includes a flake core, sidescraper, and several undiagnostic flakes (Haws et al., 2018). It is as yet unclear whether this small assemblage is part of the Early Upper Paleolithic, or possibly represents an additional Mousterian occupation. Thus the questions of Neanderthal demise in relation to HS4, and possible overlap between Middle and Upper Paleolithic industries, are currently unresolved at the site.

The sequence of levels FF-GG-HH-II (35.2–38.5 cal ka BP) appears to correspond with the prominent discontinuity noted at

many Iberian sites around the time of HS4 (Aubry et al., 2001; Galvan et al., 2014; Mallol et al., 2012). We interpret these levels as representing intense cold and dry conditions during HS4 (large clasts and low MS values in GG), followed by the return of mild humid conditions with deposition of calcite cement (mostly in GG), and muddy fine sediment and organic matter (in FF). Accompanying a sharp rise in MS values between levels GG to FF, increases in organic matter and phosphorous content suggest a warmer environment with more abundant fauna following HS4 (Figures 9–11). The cemented levels GG-II appear to correspond to a discontinuous flowstone in the uppermost Mousterian layers at nearby Gruta da Oliveira (Almonda karst network), which radiocarbon and U-series ages suggest was deposited during HS4 (Angelucci & Zilhão, 2009; Hoffmann et al., 2013). It seems likely that while some open-air sites and deeper/wetter cave systems experienced erosion or dissolution during the post-HS4 arid to humid phase, in the relatively shallow epikarst of Lapa do Picareiro the effect was limited to deposition of calcite cement across the floor of the cave while sedimentation of muddy éboulis continued.

Overall, this study demonstrates good stratigraphic completeness and integrity for the sedimentary fill of Lapa do Picareiro. The results show fairly continuous deposition through MIS 2–3-4, possibly the longest and most complete cave sequence in Portugal. The sequence contains no major erosional unconformities or large-scale diagenetic alteration. Bone, charcoal, and lithic preservation throughout the cave sequence is good. Bioturbation (by root penetration and animal burrows) is evident in the levels that have been excavated near the cave opening, but the sections studied in the cave interior appear to be intact. The cave setting (shallow karst in a ridgetop location) and morphology (a single large, deep chamber) have combined to provide a favorable environment for long-term accumulation of sediments by mainly colluvial processes and preservation of faunal, lithic, and other archaeological records.

5.3 | Paleoclimate interpretation and implications

The suitability of cave sediments as paleoenvironmental archives is broadly dependent on the temporal resolution of the sampled section and the sensitivity of the depositional system (Woodward & Goldberg, 2001). Given sedimentation rates of 0.09–0.26 mm a^{-1} for Lapa do Picareiro (Figure 7), the sampling interval of 10 cm for most of the reference profile data presented above yields a resolution of roughly 300–1,100 years between consecutive samples. The MS data, sampled at (mostly) 2 cm intervals, have a finer resolution of about 80–220 years between samples. These values are close to the threshold necessary to detect high-frequency climate fluctuations of MIS 2–3, such as Heinrich stadials that had a duration of roughly 200–2,000 years (Hemming, 2004). The sensitivity of parameters reported in this study to climate change appears to be quite variable. A few parameters, including % gravel, median large clast size, and MS appear to match the periodicity of rapid climate fluctuations during MIS 2–3-4 (Figure 13). Some compositional parameters (LOI, C:N ratios, $\delta^{13}C$ values, concentrations of Ca and Sr) are strongly influenced by the accumulation of calcitic ash and organic matter in hearths (e.g., Levels E-F) or by secondary carbonate deposition (e.g., Level GG), masking any systematic climate signal. Other parameters (fine sediment particle size, concentrations of Fe and Al) show very conservative variations with depth, seeming to reflect stable sediment sources and pathways over time regardless of climate.

Sedimentary parameters with the most apparent climate sensitivity (MS, large clast size, % gravel content, and phosphate expressed as % P_2O_5/TiO_2) are plotted against age for comparison with regional paleoenvironmental proxies over the period 9–79 ka (Figure 13). Proxies shown include the NGRIP Greenland ice core record (Rasmussen et al., 2014), summer sea surface temperature reconstructed from foraminifera in deep-sea sediment core MD95–2040 off central Portugal (Salgueiro et al., 2010), and semidesert pollen from core MD95–2042 off southern Portugal (Daniau et al., 2007). The GICC05 extended time scale used here for the NGRIP record (Svensson et al., 2008) has been shown to closely match the timing of paleoclimate transitions in proxy records for Iberia as established in offshore sediment cores (Sánchez-Goñi & Harrison, 2010; Wolff, Chappellaz, Blunier, Rasmussen, & Svensson, 2010). These and other proxies clearly show that HS episodes were times of bitterly cold temperature, aridity, and forest die-back in Portugal (Sánchez Goñi et al., 2008; Fletcher et al., 2010).

The radiocarbon-based age model presented earlier (Figure 7) provides direct age control for the stratigraphic section above 7.5 mbd (45 ka). The MS record in this section compares very favorably with paleoclimate proxy records: HS1–4 correlate closely with prolonged MS minima (levels I-J, T, Y, GG), and nearly all Greenland interstadials (GI) are represented by sharp MS peaks (Figure 13). The cold/dry Heinrich stadials correspond broadly to coarse éboulis beds with little fine sediment (high gravel content) in one or both of the reference profiles. Each of the Heinrich stadials is followed by muddy beds with elevated phosphate, which likely reflects increased fine sediment deposition and faunal activity after the return of humid climate conditions. The completeness of the MS record suggests that fine sediment deposition in the cave was fairly continuous and roughly synchronous with the accumulation of bones and charcoal that make up the radiocarbon chronology. The coarse sediment fraction, while demonstrating a periodicity that implies a paleoclimate control, represents paleoclimate events less faithfully and seems to be, at least partly, out of phase with the ages indicated by the deposition model. This likely reflects the inherent spatial and temporal discontinuities associated with weathering and deposition of éboulis clasts. For example, Level Y is a prominent coarse-clast bed with a radiocarbon age matching the early part of HS3 (Table 1). Due to within-bed variations, Level Y plots as a coarse-clast bed during HS3 in reference profile 2, but it does not appear as a coarse bed in reference profile 1 (Figure 13).

Below the radiocarbon-dated section (>7.5 mbd), the close match between the MS signal and paleoclimate record begins to break down. For this section we use a linear age model (Figure 7, Scenario b) based on matching HS6 to a strong MS minimum and coarse

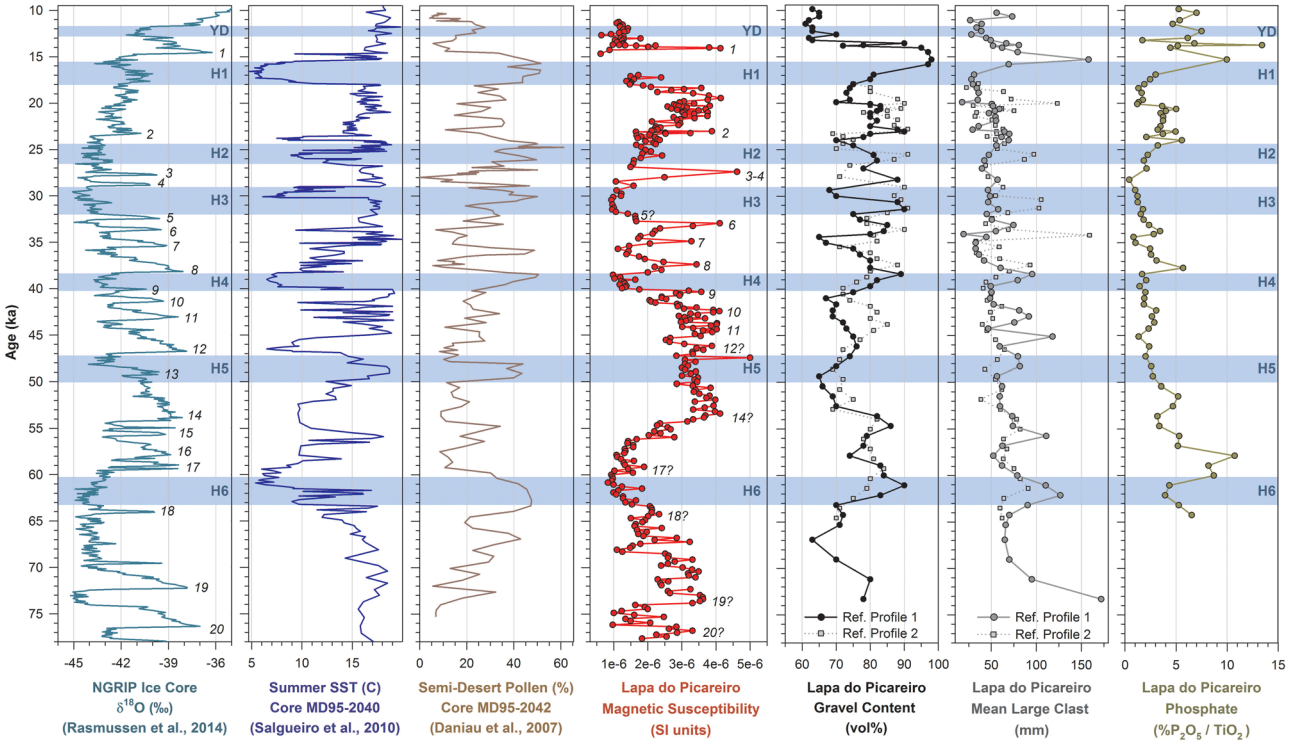

FIGURE 13 Comparison of regional climate proxies with selected sediment properties from Lapa do Picareiro from 9 to 78 ka. Picareiro data from reference profile 1 are plotted on the radiocarbon-based age model shown in Figure 7 (Scenario b). NGRIP $\delta^{18}O$ data are plotted as 100-year averages on the GICC05 extended time scale (Svensson et al., 2008; Wolff et al., 2010). Summer sea surface temperature (SST) and % semidesert pollen (Artemisia, Chenopodiaceae, Ephedra) are from sediment cores off the coast of Iberia as described in Salgueiro et al. (2010) and Daniau et al. (2007). Timing of Heinrich stadials H1-H5 from Haws (2012), H6 from Sánchez-Goñi & Harrison (2010) [Color figure can be viewed at wileyonlinelibrary.com]

éboulis bed in level LL (Figure 13). This model is based on linear extrapolation between the radiocarbon dates at 7.5 mbd (~45 ka) and the negative MS excursion beginning at 9.25 mbd, assigned to HS6 at 63.1 ka (Sánchez Goñi & Harrison, 2010). In this scenario, the sedimentation rate for the section below 7.5 mbd was around 0.09 mm a^{-1}, somewhat lower than the 0.15 mm a^{-1} rates that prevailed in overlying zones 3–4. A lower sedimentation rate in the deeper levels would reduce the resolution of the MS record and help to explain the poor match between the MS signal and paleoclimate events below GI 11 (~45 ka). Although HS6 is well-represented in this scenario, the position of HS5 remains uncertain. This pattern might be related to discrepancies in the timing and intensity of HS5 in deep-sea proxies off central and southern Portugal (sites MD-2040 and MD-2042; Sánchez Goñi et al., 2008; Fletcher et al., 2010; Salgueiro et al., 2010). The age at the base of the excavation (10.62 mbd) in the scenario described here is 77.8 ka, slightly older than the MIS 4/5 transition.

6 | CONCLUSION

Lapa do Picareiro offers a rare continuous sedimentary sequence through much of the Middle and Upper Paleolithic, in a favorable setting for long-term accumulation and preservation of sediments containing archaeological, faunal, and paleoclimatic records. The mountain top location and large-chamber morphology of the cave produced a relatively dry, passive karst environment sensitive to fluctuating climate and weathering regimes. Radiocarbon evidence establishes that sedimentation rates at the site were fairly steady (0.1–0.3 mm a^{-1}) throughout much of the Late Pleistocene. The sequence represents most or all of MIS 2, 3, and 4, including the important Middle to Upper Paleolithic transition. Deposition inside the cave ended near the beginning of the Holocene, by which time the cave mouth was nearly filled with sediment. Because no bedrock floor has yet been uncovered at the base of the excavation, the sedimentary sequence likely extends beyond the last glacial stage and into the last interglacial complex (MIS 5).

Depositional processes in the cave during the Pleistocene were dominated by the accumulation of éboulis clasts and infiltration of fine sediment derived from weathered terra rossa soils. Sediment properties suggest uniform sediment sources and limited diagenesis or biotic disturbance of the stratigraphic sequence. The sediments are variably enriched by the accumulation of secondary carbonates from anthropogenic and geogenic sources. Organic matter in the cave is mostly limited to soil organic matter decomposed by microbial activity, although bones, teeth, shell, and charcoal are locally concentrated in hearths or predator dens. Human occupation of the cave was sporadic during the Pleistocene, which together with continuous sedimentation resulted in clearly-defined cultural horizons separated by culturally-sterile but often fauna-rich levels. The

evidence recovered to date shows that human use of the cave intensified toward the top of the Upper Paleolithic, but recently-opened excavation areas are providing a more complete picture of the late Middle Paleolithic, earliest Upper Paleolithic, and transitional levels. A strong relationship exists between the MS signal in fine sediment at Picareiro and paleoclimate proxies over the radiocarbon-dated section from 9 to 45 ka. This relationship further illustrates the stratigraphic integrity of the deposits, aids in estimating the ages of undated deposits older than 45 ka and offers direct paleoenvironmental context for ongoing archaeological investigations at the site.

ACKNOWLEDGMENTS

Geoarchaeological work at Lapa do Picareiro since 2014 has been supported by collaborative research grants from the U.S. National Science Foundation, Division of Behavioral and Cognitive Sciences, to UNC Wilmington (BCS-1420453, BCS-1725015) and University of Louisville (BCS-1420299, BCS-1724997).

Our travel and research have also been supported by faculty development grants from UNC Wilmington and the University of Louisville. Student participants have been supported by Research Experiences for Undergraduates supplements to the NSF grants listed above, and from student grant support of the University of West Bohemia (SGS-2018-033). The authors thank three anonymous reviewers for suggestions that greatly improved the manuscript. We also thank the many colleagues and student assistants that have contributed to investigations at Lapa do Picareiro.

ORCID

Michael M. Benedetti http://orcid.org/0000-0002-2900-887X

REFERENCES

Aldeias, V., Dibble, H. L., Sandgathe, D., Goldberg, P., & McPherron, S. J. P. (2016). How heat alters underlying deposits and implications for archaeological fire features: A controlled experiment. *Journal of Archaeological Science*, *67*, 64–79.

Almeida, F., Moreno-Garcia, M., & Angelucci, D. E. (2009). From under the bulldozer's claws: The EE15 Late Gravettian occupation surface of the Lagar Velho rockshelter. *World Archaeology*, *21*, 242–261.

Almeida, F., Brugal, J.P., Zilhão, J., Plisson, H., Bicho, N.F. (2007). An Upper Paleolithic Pompeii: technology, subsistence andpaleoethnography at Lapa do Anecrial. From the Mediterranean basin to the Portuguese Atlantic shore: Papers in honor of Anthony Marks Actas do IV Congresso de Arqueologia Peninsular Promontória Monográfica 07, Universidade do Algarve, Faro. 119–140.

Angelucci, D. E., & Zilhão, J. (2009). Stratigraphy and formation processes of the Upper Pleistocene deposit at Gruta da Oliveira, Almonda Karstic System, Torres Novas, Portugal. *Geoarchaeology*, *24*, 277–310.

Arriolabengoa, M., Iriarte, E., Aranburu, A., Yusta, I., & Arrizabalaga, A. (2015). Provenance study of endokarst fine sediments through mineralogical and geochemical data (Lezetxiki II cave, northern Iberia). *Quaternary International*, *364*, 231–243.

Aubry, T., Fontugne, M., & Moura, M. H. (1997). Les occupations de la grotte de Buraca Grande depuis le Paléolithique supérieur et les apports de la séquence holocène à l'étude de la transition Mésolithique/Néolithique au Portugal. *Bulletin de la Société Préhistorique Française*, *94*, 182–190.

Aubry, T., Brugal, J. P., Chauviere, F. X., Figueiral, I., Moura, M. H., & Plisson, H. (2001). Modalités d'occupation au Paléolithique supérieur dans la grotte de Buraca Escura (Redinha, Pombal, Portugal). *Revista Portuguesa de Arqueologia*, *4*, 19–46.

Aubry, T., Dimuccio, L. A., Almeida, M., Neves, M. J., Angelucci, D. E., & Cunha, L. (2011). Palaeoenvironmental forcing during the Middle-Upper Palaeolithic transition in central-western Portugal. *Quaternary Research*, *75*, 66–79.

Bailey, G. N., & Woodward, J. C. (1997). The Klithi deposits: Sedimentology, stratigraphy and chronology. In G. N. Bailey (Ed.), *Klithi: Palaeolithic Settlement and Quaternary landscapes in Northwest Greece, i. excavation and intra-site analysis at Klithi* (pp. 61–94). Cambridge: McDonald Institute for Archaeological Research.

Banks, W. E. (2015). Constructing chronologies for the late Middle Paleolithic and Upper Paleolithic: Limitations and means to overcome them. *World Archaeology*, *47*, 585–600.

Bar-Yosef, O. (1993). Site formation processes from a Levantine viewpoint. In P. Goldberg, D. T. Nash, & M. D. Petraglia (Eds.), *Formation Processes in Archaeological Context*, *Monographs in World Archaeology No* 17, pp. 13–32). Madison, Wisconsin: Prehistory Press.

Bar-Yosef, O., Vandermeersch, B., Arensburg, B., Belfer-Cohen, A., Goldberg, P., Laville, H., … Weiner, S. (1992). The excavations in Kebara Cave, Mt. Carmel. *Current Anthropology*, *33*, 497–550.

Bataille, G., Tafelmaier, Y., & Weniger, G. C. (2018). Living on the edge – a comparative approach for studying the beginning of the Aurignacian. *Quaternary International*, *474*, 3–29.

Benedetti, M. M., & Haws, J. A. (2016). Geoarchaeology of Lapa do Picareiro: Linking the sedimentological, paleoenvironmental, and cultural chronologies from a Paleolithic cave site in Portugal. *Geological Society of America Abstracts with Programs*, 48. https://doi.org/10.1130/abs/2016AM-284654

Berger, G. W., Perez-Gonzalez, A., Carbonell, E., Arsuaga, J. L., Bermudez de Castro, J. M., & Ku, T. L. (2008). Luminescence chronology of cave sediments at the Atapuerca paleoanthropological site, Spain. *Journal of Human Evolution*, *55*, 300–311.

Bermudez de Castro, J. M., Martinon-Torres, M., Carbonell, E., Sarmiento, S., Rosas, A., van der Made, J., & Lozano, M. (2004). The Atapuerca sites and their contribution to the knowledge of human evolution in Europe. *Evolutionary Anthropology*, *13*, 25–41.

Bernaldo de Quiros, F., Maillo-Fernandez, J. M., Castaños, P., & Neira, A. (2015). The Gravettian of El Castillo revisited (Cantabria, Spain). *Quaternary International*, *360*, 462–478.

Bi, X., Sheng, G., Liu, X., Li, C., & Fu, J. (2005). Molecular and carbon and hydrogen isotopic composition of n-alkanes in plant leaf waxes. *Organic Geochemistry*, *36*, 1405–1417.

Bicho, N., Haws, J., & Almeida, F. (2011). Hunter-gatherer adaptations and the Younger Dryas in central and southern Portugal. *Quaternary International*, *242*, 336–347.

Bicho, N., Hockett, B., Haws, J., & Belcher, W. (2000). Hunter–gatherer subsistence at the end of the Pleistocene: Preliminary results of Picareiro Cave. *Antiquity*, *74*, 500–506.

Bicho, N., Cascalheira, J., Marreiros, J., & Pereira, T. (2017). Rapid climatic events and long term cultural change: The case of the Portuguese Upper Paleolithic. *Quaternary International*, *428*, 3–16.

Bicho, N., Manne, T., Marreiros, J., Cascalheira, J., Pereira, T., Tata, F., … Infantini, L. (2013). The ecodynamics of the first modern humans in Southwestern Iberia: The case of Vale Boi, Portugal. *Quaternary International*, *318*, 102–116.

Bicho, N. F. (2005). The extinction of Neanderthals and the emergence of the Upper Paleolithic in Portugal. *Promontoria*, *3*, 173–228.

Bicho, N. F., & Haws, J. A. (2008). At the land's end: Marine resources and the importance of fluctuations in the coastline in the prehistoric

hunter-gatherer economy of Portugal. *Quaternary Science Reviews*, *27*, 2166–2175.

Bicho, N. F., Haws, J. A., & Hockett, B. S. (2006). Two sides of the same coin: Rocks, bones and site function of Lapa do Picareiro, Central Portugal. *Journal of Anthropological Archaeology*, *25*, 485–499.

Blain, H. A., Gleed-Owen, C. P., Lopez-Garcia, J. M., Carrion, J. S., Jennings, R., Finlayson, G., … Giles-Pacheco, F. (2013). Climatic conditions for the last Neanderthals: Herpetofaunal record of Gorham's Cave, Gibraltar. *Journal of Human Evolution*, *64*, 289–299.

Blockley, S. P. E., Ramsey, C. B., & Higham, T. F. G. (2008). The Middle to Upper Paleolithic transition: Dating, stratigraphy and isochronous markers. *Journal of Human Evolution*, *55*, 764–771.

Bocherens, H., Billiou, D., Patou-Mathis, M., Bonjean, D., Otte, M., & Mariotti, A. (1997). Paleobiological implications of the isotopic signatures (13C, 15N) of fossil mammal collagen in Scladina Cave (Sclayn, Belgium). *Quaternary Research*, *48*, 370–380.

Brädtmoller, M., Pastoors, A., Weninger, B., & Weniger, G. C. (2012). The repeated replacement model: Rapid climate change and population dynamics in Late Pleistocene Europe. *Quaternary International*, *247*, 38–49.

Brock, F., Higham, T., Ditchfield, P., & Bronk Ramsey, C. (2010). Current pretreatment methods for AMS radiocarbon dating at the Oxford Radiocarbon Accelerator Unit (ORAU). *Radiocarbon*, *52*, 103–112.

Bronk Ramsey, C., Higham, T., Bowles, A., & Hedges, R. E. M. (2004). Improvements to the pretreatment of bone at Oxford. *Radiocarbon*, *46*, 155–163.

Butzer, K. W. (1981). Cave sediments, Upper Pleistocene stratigraphy and Mousterian facies in Cantabrian Spain. *Journal of Archaeological Science*, *8*, 133–183.

Carbonell, E. (Ed.), (2012). *High resolution archaeology and Neanderthal behavior: Time and space in level J of Abric Romani (Capellades, Spain)*. New York: Springer.

Carretero, J. M., Quam, R. M., Gomez-olivencia, A., Castilla, M., Rodriguez, L., & Garcia-Gonzalez, R. (2015). The Magdalenian human remains from El Miron Cave, Cantabria (Spain). *Journal of Archaeological Science*, *60*, 10–27.

Carrión, J. S., & Leroy, S. A. G. (2010). Iberian floras through time: Land of diversity and survival. *Review of Paleobotany and Palynology*, *162*, 227–230.

Carrión, J. S., Yll, E. I., Walker, M. J., Legaz, A., Chaín, C., & López, A. (2003). Glacial refugia of temperate, Mediterranean and Ibero North African flora in south-eastern Spain: New evidence from cave pollen at two Neanderthal man sites. *Global Ecology and Biogeography*, *12*, 119–129.

Carvalho, J.M.F. (2018). Jointing patterns and tectonic evolution of the Maciço Calcário Estremenho, Lusitanian Basin, Portugal. *Journal of Structural Geology*, *110*, 155–171.

Cascalheira, J., & Bicho, N. (2015). On the chronological structure of the Solutrean in Southern Iberia. *PLoS One*, *10*, e0137308.

Chester, D. K. (2001). The 1755 Lisbon earthquake. *Progress in Physical Geography*, *25*, 363–383.

Collcutt, S. N. (1979). The analysis of Quaternary cave sediments. *World Archaeology*, *10*, 290–301.

Collister, J. W., Rieley, G., Stern, B., Eglinton, G., & Fry, B. (1994). Compound-specific $\delta^{13}C$ analyses of leaf lipids from plants with differing carbon dioxide metabolisms. *Organic Geochemistry*, *21*, 619–627.

Costa, J. C., Espírito Santo, M. D., & Arsénio, P. (2010). Guide to the geobotanical excursion to the Natural Park of Serra de Aire e Candeeiros. *Quercetea*, *10*, 5–106.

Courty, M. A., & Vallverdu, J. (2001). The microstratigraphic record of abrupt climate changes in cave sediments of the Western Mediterranean. *Geoarchaeology*, *16*, 467–500.

Cucart-Mora, C., Lozano, S., & Fernandez-Lopez de Pablo, J. (2018). Bio-cultural interactions and demography during the Middle to Upper Palaeolithic transition in Iberia: An agent-based modelling approach. *Journal of Archaeological Science*, *89*, 14–24.

Cunha, S., Silva, A., Herraez, C. F., Pires, V. C., Chazarra, A., Mestre, A., … Mendes, L. (2011). *Iberian climate atlas*. Madrid: State Meteorological Agency of Spain.

Daura, J., Sanz, M., Arsuaga, J. L., Hoffmann, D. L., Quam, R. M., Ortega, M. C., … Zilhão, J. (2017). New Middle Pleistocene hominin cranium from Gruta da Aroeira (Portugal). *Proceedings of the National Academy of Sciences*, *114*, 3397–3402.

Daniau, A.-L., Sánchez-Goñi, M. F., Beaufort, L., Laggoun-Defarge, F., Loutre, M.-F., & Duprat, J. (2007). Dansgaard–Oeschger climatic variability revealed by fire emissions in southwestern Iberia. *Quaternary Science Reviews*, *26*, 1369–1383.

d'Errico, F., & Sanchez Goñi, M. F. (2003). Neanderthal extinction and the millennial scale climatic variability of OIS 3. *Quaternary Science Reviews*, *22*, 769–788.

Diefendorf, A. F., & Freimuth, E. J. (2017). Extracting the most from terrestrial plant-derived n-alkyl lipids and their carbon isotopes from the sedimentary record: A review. *Organic Geochemistry*, *103*, 1–21.

Domingo, L., Perez-Dios, P., Hernandez-Fernandez, M., Martin-Chivelet, J., Ortiz, J. E., & Torres, T. (2015). Late Quaternary climatic and environmental conditions of northern Spain: An isotopic approach based on the mammalian record from La Paloma cave. *Palaeogeography, Palaeoclimatology, Palaeoecology*, *440*, 417–430.

Douka, K., & Higham, T. (2017). The chronological factor in understanding the Middle and Upper Paleolithic of Eurasia. *Current Anthropology*, *58*, S480–S490.

Duarte, C., Maurício, J., Pettitt, P., Souto, P., Trinkaus, E., Plicht, H., & Zilhão, J. (1999). The early Upper Palaeolithic human skeleton from the Abrigo do Lagar Velho (Portugal) and modern human emergence in Iberia. *Proceedings of the National Academy of Sciences USA*, *96*, 7604–9609.

Dudal, R., Tavernier, R., & Osmond, D. (1966). *Soil map of Europe (1:2,500,000), with explanatory text*. Rome: Food and Agriculture Organization of the United Nations.

Ellwood, B. B., Zilhão, J., Harrold, F. B., Balsam, W., Burkart, B., Long, G. J., … Bouzouggar, A. (1998). Identification of the Last Glacial Maximum in the Upper Paleolithic of Portugal using magnetic susceptibility measurements of Caldeirão Cave sediments. *Geoarchaeology*, *13*, 55–71.

Ellwood, B. B., Harrold, F. B., Benoist, S. L., Straus, L. G., Morales, M. G., Petruso, K., … Soler, N. (2001). Paleoclimate and intersite correlations from Late Pleistocene/Holocene cave sites: Results from southern Europe. *Geoarchaeology*, *16*, 433–463.

Ellwood, B. B., Harrold, F. B., Benoist, S. L., Thacker, P., Otte, M., Bonjean, G., … Grandjean, F. (2004). Magnetic susceptibility applied as an age-depth-climate relative dating technique using sediments from Scladina Cave, a Late Pleistocene cave site in Belgium. *Journal of Archaeological Science*, *31*, 283–293.

Engel, A. S. (2005). Chemoautotrophy. In D. C. Culver, & W. B. White (Eds.), *The encyclopedia of caves* (pp. 90–102). New York: Elsevier.

Farrand, W. R. (1988). Integration of Late Quaternary climatic records from France and Greece: Cave sediments, pollen, and marine events. In H. L. Dibble, & A. Montet-White (Eds.), *Upper Pleistocene prehistory of western Eurasia* (pp. 305–319). Philadelphia: University of Pennsylvania.

Farrand, W. R. (2001). Archaeological sediments in rockshelters and caves. In J. K. Stein, & W. R. Farrand (Eds.), *Sediments in archaeological context* (pp. 29–66). Salt Lake City: University of Utah Press.

Finlay, J. C., & Kendall, C. (2007). Stable isotope tracing of temporal and spatial variability in organic matter sources to freshwater ecosystems. In R. Michener, & K. Lajtha (Eds.), *Stable isotopes in ecology and environmental science* 2e, pp. 283–333). Oxford: Blackwell Publishing.

Finlayson, C. (2008). On the importance of coastal areas in the survival of Neanderthal populations during the Late Pleistocene. *Quaternary Science Reviews*, *27*, 2246–2252.

Finlayson, C., & Carrion, J. S. (2007). Rapid ecological turnover and its impact on Neanderthal and other human populations. *Trends in Ecology and Evolution*, *22*, 213–222.

Finlayson, C., Giles Pacheco, F., Rodriguez-Vidal, J., Fa, D. A., Gutierrez Lopez, J. M., Santiago Perez, A., … Sakamoto, T. (2006). Late survival of Neanderthals at the southernmost extreme of Europe. *Nature*, *443*, 850–853.

Finlayson, J. C., & Giles Pacheco, F. (2000). The southern Iberian Peninsula in the late Pleistocene: Geography, ecology, and human occupation. In C. B. Stringer, R. N. E. Barton, & J. C. Finlayson (Eds.), *Neanderthals on the edge* (pp. 139–152). Oxford: Oxbow Books.

Fletcher, W. J., Goñi, M. F. S., Allen, J. R. M., Cheddadi, R., Nebout, N. C., Huntley, B., … Tzedakis, P. C. (2010). Millennial-scale variability during the last glacial in vegetation records from Europe. *Quaternary Science Reviews*, *29*, 2839–2864.

Fonseca, R. M. F., Barriga, F. J. A. S., & Conceição, P. I. S. T. (2010). Clay minerals in sediments of Portuguese reservoirs and their significance as weathering products from over-eroded soils: A comparative study of the Maranhão, Monte Novo and Divor Reservoirs (South Portugal). *International Journal of Earth Sciences*, *99*, 1899–1916.

Forbes, M. S., Bestland, E. A., Wells, R. T., & Krull, E. S. (2007). Palaeoenvironmental reconstruction of the Late Pleistocene to Early Holocene Robertson Cave sedimentary deposit, Naracoorte, South Australia. *Australian Journal of Earth Sciences*, *54*, 541–559.

Frumkin, A., Karkanas, P., Bar-Matthews, M., Barkai, R., Gopher, A., Shahack-Gross, R., & Vaks, A. (2009). Gravitational deformations and fillings of aging caves: The example of Qesem karst system, Israel. *Geomorphology*, *106*, 154–164.

Galvan, B., Hernandez, C. M., Mallol, C., Mercier, N., Sistiaga, A., & Soler, V. (2014). New evidence of early Neanderthal disappearance in the Iberian Peninsula. *Journal of Human Evolution*, *75*, 16–27.

Gamble, C. S. (1986). *The Paleolithic settlement of Europe*. Cambridge: Cambridge University Press.

García-Amorena, I., Manzaeque, F. G., Rubiales, J. M., Granja, H. M., Carvalho, G. S., & Morla, C. (2007). The Late Quaternary forests of western Iberia: A study of their macroremains. *Palaeogeography, Palaeoceanography, Palaeoecology*, *254*, 448–461.

Gleixner, G. (2013). Soil organic matter dynamics: A biological perspective derived from the use of compound-specific isotopes studies. *Ecological Research*, *28*, 683–695.

Goldberg, P., & Sherwood, S. C. (2006). Deciphering human prehistory through the geoarcheological study of cave sediments. *Evolutionary Anthropology*, *15*, 20–36.

Goldberg, P., Laville, H., & Meignen, L. (2007). Stratigraphy and geoarchaeological history of Kebara Cave, Mount Carmel. In O. Bar-Yosef, & L. Meignen (Eds.), *Kebara Cave, Part 1* (pp. 49–89). Cambridge: Peabody Museum of Archaeology and Ethnology, Harvard University.

Goldberg, P., Dibble, H., Berna, F., Sandgathe, D., McPherron, S. J. P., & Turq, A. (2012). New evidence on Neandertal use of fire: Examples from Roc de Marsal and Pech de l'Aze IV. *Quaternary International*, *247*, 325–340.

Gonzalez-Samperiz, P., Leroy, S. A. G., Carrion, J. S., Fernandez, S., Garcia-Anton, M., Gil-Garcia, M. J., … Figueiral, I. (2010). Steppes, savannahs, forests and phytodiversity reservoirs during the Pleistocene in the Iberian Peninsula. *Review of Paleobotany and Palynology*, *162*, 427–457.

Gopher, A., Ayalon, A., Bar-Matthews, M., Barkai, R., Frumkin, A., Karkanas, P., & Shahack-Gross, R. (2010). The chronology of the later Lower Paleolithic in the Levant based on U-Th ages of speleothems from Qesem Cave, Israel. *Quaternary Geochronology*, *5*, 644–656.

Haws, J. A. (2012). Paleolithic socionatural relationships during MIS 3 and 2 in central Portugal. *Quaternary International*, *264*, 61–77.

Haws, J. A., Benedetti, M. M., Funk, C. L., Bicho, N. F., Daniels, J. M., Hesp, P., … Hockett, B. S. (2010). Coastal wetlands and the Neanderthal settlement of Portuguese Estremadura. *Geoarchaeology*, *25*, 709–744.

Haws, J., Benedetti, M., Friedl, L., Bicho, N., Cascalheira, J., & Carvalho, M. (2018). *The Middle-Upper Paleolithic transition in southern Iberia: new data from Lapa do Picareiro, Portugal*. 8th Annual Meeting of the European Society for the Study of Human Evolution, Faro, Portugal, Poster Presentation Number 11.

Herries, A. I. R. (2006). Archaeomagnetic evidence for climate change at Sibudu Cave. *South African Humanities*, *18*, 131–147.

Hemming, S. R. (2004). Heinrich events: massive late Pleistocene detritus layers of the North Atlantic and their global climate imprint. *Review of Geophysics*, *42*, RG1005.

Higham, T. (2011). European Middle and Upper Palaeolithic radiocarbon dates are often older than they look: Problems with previous dates and some remedies. *Antiquity*, *85*, 235–249.

Higham, T., Douka, K., Wood, R., Bronk Ramsey, C., Brock, F., Basell, L., … Jacobi, R. (2014). The timing and spatiotemporal patterning of Neanderthal disappearance. *Nature*, *512*, 306–309.

Hockett, B. S. (1999). Taphonomy of a carnivore-accumulated rabbit bone assemblage from Picareiro Cave, Portugal. *Journal of Iberian Archaeology*, *1*, 225–230.

Hockett, B. S., & Bicho, N. F. (2000). The rabbits of Picareiro Cave: Small mammal hunting during the Late Upper Palaeolithic in the Portuguese Estremadura. *Journal of Archaeological Science*, *27*, 715–723.

Hockett, B. S., & Haws, J. A. (2002). Taphonomic and methodological perspectives of leporid hunting during the Upper Paleolithic of the western Mediterranean Basin. *Journal of Archaeological Method and Theory*, *9*, 269–302.

Hockett, B. S., & Haws, J. A. (2005). Nutritional ecology and the extinction of the European Neandertals. *Quaternary International*, *137*, 21–34.

Hockett, B. S., & Haws, J. A. (2009). Continuity in animal resource diversity in the Late Pleistocene human diet of central Portugal, *Before Farming* 2009). Liverpool, UK: Liverpool university press.

Hoffmann, D.L., Pike, A.W.G., Wainer, K., & Zilhão, J. (2013). New U-series results for the speleogenesis and the Palaeolithic archaeology of the Almonda karstic system (Torres Novas, Portugal). *Quaternary International*, *294*, 168–182.

Iacoviello, F., & Martini, I. (2012). Provenance and geological significance of red mud and other clastic sediments of the Mugnano Cave (Montagnola Senese, Italy). *International Journal of Speleology*, *41*, 317–328.

Jimenez-Espejo, F. J., Rodriguez-Vidal, J., Finlayson, C., Martinez-Ruiz, F., Carrion, J. S., Garcia-Alix, A., … Aguirre, A. M. (2013). Environmental conditions and geomorphologic changes during the Middle–Upper Paleolithic in the southern Iberian Peninsula. *Geomorphology*, *180*, 205–216.

Jöris, O., & Street, M. (2008). At the end of the 14C time scale - the Middle to Upper Paleolithic record of western Eurasia. *Journal of Human Evolution*, *55*, 782–802.

Karkanas, P., & Goldberg, P. (2010). Site formation processes at Pinnacle Point Cave 13B (Mossel Bay, Western Cape Province, South Africa): Resolving stratigraphic and depositional complexities with micromorphology. *Journal of Human Evolution*, *59*, 256–273.

Karkanas, P., & Goldberg, P. (2016). Cave settings. In A. S. Gilbert (Ed.), *Encyclopedia of geoarchaeology* (pp. 108–118). New York: Springer.

Karkanas, P., Bar-Yosef, O., Goldberg, P., & Weiner, S. (2000). Diagenesis in prehistoric caves: The use of minerals that form in situ to assess the completeness of the archaeological record. *Journal of Archaeological Science*, *27*, 915–929.

Lalueza Fox, C., Rosas, A., & de la Rasilla, M. (2012). Palaeogenetic research at the El Sidrón Neanderthal site. *Annals of Anatomy*, *194*, 133–137.

Kim, J. Y., Krivonogov, S. K., Lee, Y. J., Woo, J. Y., Oh, K. C., Yang, D. Y., Kim, J. C., Safonova, I. Y., & Yamamoto, M. (2013). Climatic stages recorded in sediments of the Gunang Cave, South Korea. *Quaternary International*, *313*, 194–209.

Kourampas, N., Simpson, I. A., Perera, N., Deraniyagala, S. U., & Wijeyapala, W. (2009). Rockshelter sedimentation in a dynamic

tropical landscape: Late Pleistocene–Early Holocene archaeological deposits in Kitulgala Beli-lena, southwestern Sri Lanka. *Geoarchaeology*, *24*, 677–714.

Lane, C. S., Horn, S. P., Mora, C. I., & Orvis, K. H. (2009). Late-Holocene paleoenvironmental change at mid-elevation on the Caribbean slope of the Cordillera Central, Dominican Republic: A multi-site, multi-proxy analysis. *Quaternary Science Reviews*, *28*, 2239–2260.

Laville, H., Rigaud, J. P., & Sackett, J. (1980). *The rockshelters of the Perigord*. New York: Academic Press.

Lourenço, A. M., Rocha, F., & Gomes, C. R. (2012). Relationships between magnetic parameters, chemical composition and clay minerals of topsoils near Coimbra, central Portugal. *Natural Hazards and Earth System Sciences*, *12*, 2545–2555.

Macphail, R. I., & Goldberg, P. (2000). Geoarchaeological investigation of sediments from Gorham's and Vanguard Caves, Gibraltar: Micro-stratigraphical (soil micromorphological and chemical) signatures. In C. B. Stringer, R. N. E. Barton, & J. C. Finlayson (Eds.), *Neanderthals on the edge* (pp. 183–200). Oxford: Oxbow Books.

Mallol, C., Cabanes, D., & Baena, J. (2010). Microstratigraphy and diagenesis at the upper Pleistocene site of Esquilleu Cave (Cantabria, Spain). *Quaternary International*, *214*, 70–81.

Mallol, C., Hernandez, C. M., & Machado, J. (2012). The significance of stratigraphic discontinuities in Iberian Middle-to-Upper Paleolithic transitional sites. *Quaternary International*, *275*, 4–13.

Marean, C. W. (2014). The origins and significance of coastal resource use in Africa and Western Eurasia. *Journal of Human Evolution*, *77*, 17–40.

Marin-Arroyo, A. B., Rios-Garaizar, J., Straus, L. G., Jones, J. R., de la Rasilla, M., Gonzalez Morales, M. R., … Ocio, D. (2018). Chronological reassessment of the Middle to Upper Paleolithic transition and Early Upper Paleolithic cultures in Cantabrian Spain. *PLoS One*, *13*, e0194708.

Marks, A. E., Brugal, J. P., Chabai, V. P., Monigal, K., Goldberg, P., Hockett, B., … Mallol, C. (2002). Le gisement Pleistocène Moyen de Galeria Pesada (Estremadure, Portugal): Premiers resultats. *Paleo*, *14*, 77–99.

McLennan, S. M., Hemming, S., McDaniel, D. K., & Hanson, G. N. (1993). Geochemical approaches to sedimentation, provenance, and tectonics. In M.J. Johnson, & A. Basu (Eds.), *Processes controlling the composition of clastic sediments* (pp. 21–40). Boulder, CO: Geological Society of America. Special Paper 284.

Mora, R., Martinez-Moreno, J., Sunyer, M. R., Sunyer, M. R., Calvo, A. B., Polo-Diaz, A., & Carro, S. S. (2018). Contextual, technological and chronometric data from Cova Gran: Their contribution to discussion of the Middle-to-Upper Paleolithic transition in northeastern Iberia. *Quaternary International*, *474*, 30–43.

Moreno, A., Gonzalez-Samperiz, P., Morellon, M., Valero-Garces, B. L., & Fletcher, W. J. (2012). Northern Iberian abrupt climate change dynamics during the last glacial cycle: A view from lacustrine sediments. *Quaternary Science Reviews*, *36*, 139–153.

Muhs, D. R., Budahn, J., Avila, A., Skipp, G., Freeman, J., & Patterson, D. (2010). The role of African dust in the formation of Quaternary soils on Mallorca, Spainand implications for the genesis of Red Mediterranean soils. *Quaternary Science Reviews*, *29*, 2518–2543.

Morley, M. W., & Woodward, J. C. (2011). The Campanian Ignimbrite (Y5) tephra at Crvena Stijena Rockshelter, Montenegro. *Quaternary Research*, *75*, 683–696.

Naughton, F., Sanchez Goñi, M. F., Kageyama, M., Bard, E., Duprat, J., Cortijo, E., … Turon, J. L. (2009). Wet to dry climatic trend in north-western Iberia within Heinrich events. *Earth and Planetary Science Letters*, *284*, 329–342.

O'Leary, M. H. (1981). Carbon isotope fractionation in plants. *Phytochemistry*, *20*, 553–567.

Pereira, T., & Benedetti, M. (2013). A model for raw material management as a response to local and global environmental constraints. *Quaternary International*, *318*, 19–32.

Peterson, B. J., & Fry, B. (1987). Stable isotopes in ecosystem studies. *Annual Review of Ecology and Systematics*, *18*, 293–320.

Pohlman, J. W., Iliffe, T. M., & Cifuentes, L. A. (1997). A stable isotope study of organic cycling and the ecology of an anchialine cave system. *Marine Ecology Progress Series*, *155*, 17–27.

Polo-Diaz, A., Benito-Calvo, A., Martinez-Moreno, J., & Mora Torcal, R. (2016). Formation processes and stratigraphic integrity of the Middle-to-Upper Palaeolithic sequence at Cova Gran de Santa Linya (South-eastern Prepyrenees of Lleida, Iberian Peninsula). *Quaternary International*, *417*, 16–38.

Presleyer, J., Carrion, E., Cuartero, F., & Fluck, H. (2012). A chronicle of crisis: The Late Mousterian in north Iberia (Cueva del Esquilleu, Cantabria, Spain). *Quaternary International*, *247*, 199–211.

Reimer, P. J., Bard, E., Bayliss, A., Beck, J. W., Blackwell, P. G., Ramsey, C. B., … van der Plicht, J. (2013). IntCal13 and Marine13 radiocarbon age calibration curves 0–50,000 years cal BP. *Radiocarbon*, *55*, 1869–1887.

Rasmussen, S.O., Bigler, M., Blockley, S. P., Blunier, T., Buchardt, S. L., Clausen, H. B., Cvijanovich, I., Dahl-Jensen, D., Johnsen, S. J., Fischer, H., Gkinis, V., Guillevic, M., Hoek, W. Z., Lowe, J. J., Pedro, J. B., Popp, T., Seierstad, I. K. , Steffensen, J. P., Svensson, A. M., Vallelonga, P., Vinther, B. M., Walker, M. J. C., Wheatley, J. J. , & Winstrup, M. (2014). A stratigraphic framework for abrupt climatic changes during the LastGlacial period based on three synchronized Greenland ice-corerecords: refining and extending the INTIMATE event stratigraphy. *Quaternary Science Reviews*, *106*, 14–28.

Rocha, F. J. F. T., & Gomes, C. S. F. (1996). Discrimination of Tertiary and Quaternary lithostratigraphic units in the Aveiro region on the basis of clay minerals. *Acta Universitatis Carolinae*, *Geologica*, *38*, 381–390.

Rosas, A., Martínez Maza, C., Bastir, M., Garci Tabernero, A., Lalueza Fox, C., Huguet, R., … Fortea, J. (2006). Paleobiology and comparative morphology of a late Neandertal sample from El Sidrón, Asturias, Spain. *Proceedings of the National Academy of Sciences*, *103*, 19266–19271.

Roucoux, K. H., de Abreu, L., Shackleton, N. J., & Tzedakis, P. C. (2005). The response of NW Iberian vegetation to North Atlantic climate oscillations during the last 65 kyr. *Quaternary Science Reviews*, *24*, 1637–1653.

Salgueiro, E., Voelker, A. H. L., Abreu, Ld, Abrantes, F., Meggers, H., & Wefer, G. (2010). Temperature and productivity changes off the western Iberian margin during the last 150 ky. *Quaternary Science Reviews*, *29*, 680–695.

Sánchez Goñi, M. F., & Harrison, S. P. (2010). Millennial-scale climate variability and vegetation changes during the Last Glacial: Concepts and terminology. *Quaternary Science Reviews*, *29*, 2823–2827.

Sánchez Goñi, M. F., Landais, A., Fletcher, W. J., Naughton, F., Desprat, S., & Duprat, J. (2008). Contrasting impacts of Dansgaard-Oeschger events over a western European latitudinal transect modulated by orbital parameters. *Quaternary Science Reviews*, *27*, 1136–1151.

Sanudo, P., Blasco, R., & Fernandez Peris, J. (2016). Site formation dynamics and human occupations at Bolomor Cave (Valencia, Spain): An archaeostratigraphic analysis of levels I to XII (100-200 ka). *Quaternary International*, *417*, 94–104.

Sarbu, S. M., Kane, T. C., & Kinkle, B. K. (1996). A chemautotrophically based cave system. *Science*, *272*, 1953–1955.

Schmidt, I., Bradtmöller, M., Kehl, M., Pastoors, A., Tafelmaier, Y., Weninger, B., & Weniger, G. C. (2012). Rapid climate change and variability of settlement patterns in Iberia during the Late Pleistocene. *Quaternary International*, *271*, 179–204.

Shahack-Gross, R., Ayalon, A., Goldberg, P., Goren, Y., Ofek, B., Rabinovich, R., & Hovers, E. (2008). Formation processes of cemented features in karstic cave sites revealed using stable oxygen and carbon isotopic analyses: A case study at Middle Paleolithic Amud Cave, Israel. *Geoarchaeology*, *23*, 43–62.

Skaberne, D., Turk, I., & Turk, J. (2015). The Pleistocene clastic sediments in the Divje babe I cave, Slovenia. Palaeoclimate (part 1). *Palaeogeography*, *Palaeoclimatology*, *Palaeoecology*, *438*, 395–407.

Soil Survey Staff (1999). *Soil taxonomy: A basic system of soil classification for making and interpreting soil surveys* (2nd ed, 436. Washington, D.C.: U.S. Department of Agriculture, Natural Resources Conservation Service.

Still, C. J., Berry, J. A., Collatz, G. J., & DeFries, R. S. (2003). Global distribution of C_3 and C_4 vegetation: Carbon cycle implications. *Global Biogeochemical Cycles*, *17*, 1006–6-14.

Straus, L. G. (2013). Iberian archaeofaunas and hominin subsistence during Marine Isotope Stages 4 and 3. In J. L. Clark, & J. D. Speth (Eds.), *Zooarchaeology and modern human origins: human hunting behavior during the later Pleistocene* (pp. 97–128). Dordrecht: Springer.

Straus, L. G. (2015). Recent developments in the study of the Upper Paleolithic of Vasco-Cantabrian Spain. *Quaternary International*, *364*, 255–271.

Straus, L. G., Bicho, N., & Winegardner, A. C. (2000). The Upper Paleolithic settlement of Iberia: First-generation maps. *Antiquity*, *74*, 553–566.

Stringer, C. B., Finlayson, J. C., Barton, R. N. E., Fernandez-Jalvo, Y., Caceres, I., Sabin, R. C., … Riquelme-Cantal, J. A. (2008). Neanderthal exploitation of marine mammals in Gibraltar. *Proceedings of the National Academy of Sciences*, *105*, 14319–14324.

Svensson, A., Andersen, K. K., Bigler, M., Clausen, H. B., Dahl-Jensen, D., Davies, S. M., … Vinther, B. M. (2008). A 60000 year Greenland stratigraphic ice core chronology. *Climate of the Past*, *4*, 47–57.

Talamo, S., & Richards, M. (2011). A comparison of bone pretreatment methods for AMS dating of sample >30,000 BP. *Radiocarbon*, *53*, 443–449.

Taylor, A. K., Benedetti, M. M., Haws, J. A., & Lane, C. S. (2017). Mid-Holocene Iberian hydroclimate variability and paleoenvironmental change: Molecular and isotopic insights from Praia Rei Cortiço, Portugal. *Journal of Quaternary Science*, *33*, 79–92.

Talamo, S., Hughen, K. A., Kromer, B., & Reimer, P. J. (2012). Debates over Palaeolithic chronology - the reliability of 14C is confirmed. *Journal of Archaeological Science*, *39*, 2464–2467.

de la Torre, I., Martinez-Moreno, J., & Mora, R. (2013). Change and stasis in the Iberian Middle Paleolithic: Considerations on the significance of Mousterian technological variability. *Current Anthropology*, *54*, S320–S336.

Trinkaus, E., Walker, M. J. (2017). *The people of Palomas: Neandertals from the Sima de las Palomas del Cabezo Gordo, southeastern Spain*. College Station, TX: Texas A&M University Press. Series, 19.

Trinkaus, E., Maki, J., & Zilhão, J. (2007). Middle Paleolithic human remains from the Gruta da Oliveira (Torres, Novas), Portugal. *American Journal of Physical Anthropology*, *134*, 263–273.

Turk, J., & Turk, M. (2010). Paleotemperature record in late Pleistocene clastic sediments at Divje Babe 1 cave (Slovenia). *Journal of Archaeological Science*, *37*, 3269–3280.

Turon, J. L., Lezine, A. M., & Denefle, M. (2003). Land-sea correlations for the last glaciation inferred from a pollen and dinocyst record from the Portuguese margin. *Quaternary Research*, *59*, 88–96.

Tzedakis, P. C., Hughen, K. A., Cacho, I., & Harvati, K. (2007). Placing late Neanderthals in a climatic context. *Nature*, *449*, 206–208.

Vautravers, M. J., & Shackleton, N. J. (2006). Centennial-scale surface hydrology off Portugal during Marine Isotope Stage 3, insights from planktonic foraminiferal fauna variability. *Paleoceanography*, *21*. PA3004

Weiner, S. (2010). *Microarchaeology: Beyond the visible archaeological record*. New York, NY: Cambridge University Press.

White, W. B. (2007). Cave sediments and paleoclimate. *Journal of Cave and Karst Studies*, *69*, 76–93.

Wolff, E. W., Chappellaz, J., Blunier, T., Rasmussen, S. O., & Svensson, A. (2010). Millennial-scale variability during the last glacial: The ice core record. *Quaternary Science Reviews*, *29*, 2828–2838.

Wood, R. E., Barroso-Ruiz, C., Caparros, M., Pardo, J. F. J., Santos, B. G., & Higham, G. F. G. (2013). Radiocarbon dating casts doubt on the late chronology of the Middle to Upper Palaeolithic transition in southern Iberia. *Proceedings of the National Academy of Sciences*, *110*, 2781–2786.

Wood, R. E., Arrizabalaga, A., Camps, M., Fallon, S., Iriarte-Chiapusso, M. J., Jones, R., … Higham, T. F. G. (2014). The chronology of the earliest Upper Palaeolithic in northern Iberia: New insights from L'Arbread, Labeko Koba, and La Viña. *Journal of Human Evolution*, *69*, 91–109.

Woodward, J. C. (1997). Late Pleistocene rockshelter sedimentation at Megalakkos. In G. N. Bailey (Ed.), *Klithi: Palaeolithic Settlement and Quaternary Landsapes in Northwest Greece* 2, pp. 377–393). Cambridge: McDonald Institute for Archaeological Research.

Woodward, J. C., & Bailey, G. N. (2000). Sediment sources and terminal Pleistocene geomorphological processes recorded in rockshelter sequences in Northwest Greece. In I. D. L. Foster (Ed.), *Tracers in Geomorphology* (pp. 521–551). Chichester: Wiley.

Woodward, J. C., & Goldberg, P. (2001). The sedimentary records in Mediterranean rockshelters and caves: Archives of environmental change. *Geoarchaeology*, *16*, 465–466.

Woodward, J. C., Hamlin, R. H. B., Macklin, M. G., Karkanas, P., & Kotjabopoulou, E. (2001). Quantitative sourcing of slackwater deposits at Boila rockshelter: A record of lateglacial flooding and Paleolithic settlement in the Pindus Mountains, Northwest Greece. *Geoarchaeology*, *16*, 501–536.

Zilhão, J. (2000). Nature and culture in Portugal from 30,000 to 20,000 BP. In W. Roebroeks, M. Mussi, J. Svoboda, & K. Fennema (Eds.), *Hunters of the golden age: The Mid-Upper Paleolithic of Eurasia 30,000-20,000 BP* (pp. 337–354). Leiden: Leiden University Press.

Zilhão, J. (2006). Chronostratigraphy of the Middle-to-Upper Paleolithic transition in the Iberian Peninsula. *Pyrenae*, *37*, 7–84.

Zilhão, J. (2013). Seeing the leaves and not missing the forest: A Portuguese perspective of the Solutrean. In A. Pastoors, & B. Auffermann (Eds.), *Pleistocene foragers on the Iberian Peninsula: their culture and environment* (pp. 201–216). Mettmann: Neanderthal Museum.

Zilhão, J., & Almeida, F. (2002). The archeological framework. In J. Zilhão, & E. Trinkaus (Eds.), *Portrait of the artist as a child: The Gravettian human skeleton from the Abrigo do Lagar Velho and its archaeological context. Trabalhos de Arqueologia* 22, pp. 29–57). Lisboa: Instituto Portugûes de Arqueologia.

Zilhão, J., Davis, S. J. M., Duarte, C., Soares, A. M. M., Steier, P., & Wild, E. (2010). Pego do Diabo (Loures, Portugal): Dating the emergence of anatomical modernity in westernmost Eurasia. *PLoS One*, *5*, e8880.

Zilhão, J., Ajas, A., Badal, E., Burow, C., Kehl, M., López-Sáez, J. A., … Zapata, J. (2016). Cueva Antón: A multi-proxy MIS 3 to MIS 5 paleoenvironmental record for SE Iberia. *Quaternary Science Reviews*, *146*, 251–273.

Zilhão, J., Anesin, D., Aubry, T., Badal, E., Cabanes, D., Kehl, M., … Zapata, J. (2017). Precise dating of the Middle-to-Upper Paleolithic transition in Murcia (Spain) supports late Neandertal persistence in Iberia. *Heliyon*, *3*, e00435.

How to cite this article: Benedetti MM, Haws JA, Bicho NF, Friedl L, Ellwood BB. Late Pleistocene site formation and paleoclimate at Lapa do Picareiro, Portugal. *Geoarchaeology*. 2019;1–29. https://doi.org/10.1002/gea.21735